Cholesterol lowering depletes atherosclerotic lesions of smooth muscle cell-derived fibromyocytes and chondromyocytes

Laura Carramolino[1], Julián Albarrán-Juárez[2], Anton Markov[2], Esther Hernández-SanMiguel[1], Diana Sharysh[2], Vanessa Cumbicus[1], Daniel Morales-Cano[1,2], Veronica Labrador-Cantarero[1], Peter Loof Møller[3], Paula Nogales[1], Alberto Benguria[1], Ana Dopazo[1,4], Fátima Sanchez-Cabo[1], Carlos Torroja[1], Jacob F. Bentzon[1,2,5,6*]

[1]Centro Nacional de Investigaciones Cardiovasculares (CNIC), Madrid, Spain
[2]Atherosclerosis Research Unit, Department of Clinical Medicine, Aarhus University, Aarhus, Denmark
[4]Department of Biomedicine, Aarhus University, Aarhus, Denmark
[4]CIBER de Enfermedades Cardiovasculares, Madrid, Spain.
[5]Steno Diabetes Center Aarhus, Aarhus University Hospital, Aarhus, Denmark
[6]Department of Cardiology, Aarhus University Hospital, Aarhus, Denmark

*Address for correspondence
Jacob F. Bentzon
Atherosclerosis Reseach Unit,
Department of Clinical Medicine, Aarhus University
A503, Palle Juul-Jensens Boulevard 11,
8200 Aarhus N
Denmark
Email: jfbentzon@clin.au.dk

Abstract

Drugs that lower plasma ApoB-containing lipoproteins are central to treating advanced atherosclerosis and provide partial protection against clinical events. Previous research showed that lowering ApoB-containing lipoproteins stops plaque inflammation, but how these drugs affect the heterogeneous population of plaque cells derived from smooth muscle cells (SMCs) is unknown. SMC-derived cells are the main cellular component of atherosclerotic lesions and the source of structural components that determine the size of plaques and their propensity to rupture and trigger thrombosis, the proximate cause of heart attack and stroke. Using lineage tracing and single-cell techniques to investigate the full SMC-derived cellular compartment in progressing and regressing plaques in mice, here we show that lowering ApoB-containing lipoproteins reduces NFκB signaling in SMC-derived fibromyocytes and chondromyocytes and leads to depletion of these abundant cell types from plaques. These results uncover an important mechanism through which cholesterol-lowering drugs can achieve plaque regression.

Main text

ApoB-containing lipoproteins (ApoB-LPs) cause atherosclerotic lesions to progress and culminate in heart attack and stroke;[1] however, reducing plasma ApoB-LP levels through the use of statins, ezetimibe, or PCSK9 inhibitors (typically measured by a reduction in plasma cholesterol) is not always sufficient to halt disease activity in patients with advanced atherosclerosis. There is an important need to define the mechanisms by which ApoB-LP lowering exerts its protective effect within plaques to identify paths to enhancing treatment efficacy and achieving faster disease remission. An important example of this strategy is that previous studies showed that ApoB-LP lowering leads to rapid resolution of plaque inflammation,[2–6] and potentiation of this anti-inflammatory effect with anti-IL1β antibodies or colchicine increases protection against atherosclerotic clinical events in high-risk patients.[7,8]

It remains unclear whether the large population of plaque cells deriving from smooth muscle cells (SMCs) mediate part of the beneficial effect of ApoB-LP lowering. During mouse and human atherosclerosis, local SMCs proliferate and modulate to a range of SMC-derived phenotypes, including cells with characteristics of fibroblasts (fibromyocytes) and osteochondrogenic cells (chondromyocytes).[9–14] Many of these cells also become foam cells engorged with cholesteryl esters.[11,15] SMCs have a recognized beneficial role in forming the fibrous cap that protects the plaque surface from rupturing and precipitating a thrombus; however, some SMC-derived cells can be detrimental and drive plaque growth.[16] Previous studies have not addressed whether ApoB-LP lowering leads to changes in the abundance, subtypes, or functions of SMC-derived cells, but this is of high interest since these populations are major determinants of plaque vulnerability and plaque size and may be targets for supplementary drug therapy.

Here, we combined mouse models of SMC lineage tracing, ApoB-LP-altering techniques, and single-cell expression profiling to analyze the phenotypic diversity and gene expression of SMC-derived cells in progressing and regressing plaques. We found that lowering ApoB-LPs leads to early reversal of NFκB signaling in SMC-derived fibromyocytes and chondromyocytes followed by their depletion from plaques, while contractile cap SMC numbers remain stable.

Results

ApoB-LP lowering resolves plaque inflammation

To trace SMCs and their progeny in response to ApoB-LP lowering, we utilized Myh11-CreER^{T2} x TdTomato (TdT) reporter mice, administering tamoxifen at 6 weeks of age. Atherosclerotic lesions were induced by injection of PCSK9^{D377Y}-encoding adeno-associated virus at 10 weeks of age, followed by 16 weeks of a high-fat diet. For a further 4 weeks, mouse groups were either maintained on the high-fat diet (HF group, n=9), transitioned to a low-fat diet to achieve moderately low plasma ApoB-LP levels (4wLF group, n=13), or shifted to the low-fat diet plus weekly injections of *Apob* mRNA-targeting antisense oligonucleotides to achieve very low ApoB-LP levels (4wLF/ASO group, n=14). The interventions effectively reduced plasma total and ApoB-LP cholesterol, triglycerides, and, to a lesser extent, HDL cholesterol (**Fig. 1a** and **Extended Data Fig. 1a**).

Aortic root plaques were moderately smaller in 4wLF and 4wLF/ASO mice than in HF mice and had a substantially lower content of Oil Red O-stained neutral lipids, which in plaques are mainly cholesteryl esters (**Fig. 1b**).[17] There were no significant changes in fibrotic components (stained with Sirius Red) or necrotic core area. Analysis of cellular composition showed the expected reduction in plaque macrophages in 4wLF and 4wLF/ASO mice (**Fig. 1c-f**). Macrophages were defined as CD68+TdT- cells to exclude a small fraction of SMC-derived cells that express CD68. A theoretically superior pan-macrophage marker, TYROBP,[18] which also markedly decreased by ApoB-LP lowering (**Fig. 1d,f**). In contrast, SMC-derived cells (TdT+) were maintained at high numbers (50%-70%) in all groups with only a minor and statistically insignificant decline observed after 4 weeks of ApoB-LP lowering (**Fig. 1g**).

Phenotypic diversity of the SMC-derived cells

Because the SMC-derived cell population is heterogeneous, we next asked if 4 weeks of ApoB-LP lowering changes the distribution of cell subtypes. We first conducted a single-cell RNA sequencing (scRNA-seq) analysis of pooled tissue from atherosclerotic aortic arches (stripped of adventitia) obtained from new groups of HF mice (n=6) and 4wLF/ASO mice (n=7). Dimensionality reduction and clustering separated cells into endothelial cells (positive for *Cdh5*), macrophages (positive for *Cd68* and *Tyrobp*), and SMC-derived cells (positive for the TdT transcript) (**Fig. 2a-b** and **Extended Data Fig. 2a-d**). Some data points with TdT expression clustered with macrophages and endothelial cells, but many of these cases also expressed markers of highly differentiated SMCs (eg. *Myh11*, **Extended Data Fig. 2e**), suggesting that they were cell doublets, a known artefact in scRNA-seq data, and not SMCs transforming to macrophage- or endothelial-like cells. Applying an algorithm to identify cell doublets[19] largely explained the occurrence of these mixed-identity signals (**Fig. 2c**). Further analysis was therefore performed with data rigorously filtered for doublets and without the endothelial and macrophage clusters.

Re-clustering of SMC-derived cells at moderate resolution divided them into 5 subclusters, which we characterized according to their top marker genes (genes with significantly higher expression than in all other clusters), and named them according to a modification of the nomenclature introduced by Quertermous and colleagues (**Fig. 2d-e** and **Supplementary Table 1**).[13] The main axis of phenotypic diversity spanned from conventional SMCs expressing contractile genes (eg. *Acta2*, *Myh11*) in cluster C0 (named *SMC0*), through cells with a fibroblast-like phenotype and showing evidence of inflammatory signaling (eg. *Lum*, *Ly6a*, *Vcam1*) in cluster C1 (named *fibromyocytes*), to cells with a gene-expression profile resembling that of chondrocytes (eg. *Sox9*, *Col2a1*) in cluster C2 (*chondromyocytes*). Two additional subclusters were identified among cells expressing contractile genes: one with intermediate contractile gene expression and expression of the pericyte marker *Rgs5* in cluster C3 (*SMC1*), and another with high contractile gene expression and evidence of cell stress

pathway activation (eg. *Atf3, Fos*) in cluster 4 (*SMC2*). The marker gene signature of the latter corresponds to a dissociation gene signature described in other tissues.[20] The cellular diversity was consistent with other published scRNA-seq data sets from mouse atherosclerotic plaques (**Extended Data Fig.2f**).[12,13,21,22]

To understand what drives these phenotypic differences, we performed an analysis by single-cell regulatory network inference and clustering (SCENIC) (**Fig. 2f**), a strategy that identifies regulation of regulons based on co-expression of genes with transcription factors and an analysis of cis-regulatory motifs.[23] Clusters expressing contractile genes (SMC0-2) showed evidence for gene regulatory programs driven by Srf, Mef2c, and Notch signaling (Heyl), which are important regulators of SMC phenotype. The small SMC2 subcluster had multiple additional gene regulatory programs driven by stress- and inflammation-regulating transcription factors. At the other end of the spectrum, chondromyocytes showed a profoundly different gene regulation, with upregulation of Sox9- and Runx1-driven regulons (implicated in chondrocyte differentiation) and hypoxia-driven genes (Hif1a regulon), together with evidence of increased NFκB signaling (Rel, Relb, Nfkb1, and Nfkb2 regulons). Fibromyocytes had intermediate upregulation of Srf and Sox9/Runx1 regulons but lacked evidence of specific gene regulatory programs not shared with either contractile SMCs or chondromyocytes.

ApoB-LP lowering reduces fibromyocytes and chondromyocytes

Based on the scRNA-seq and SCENIC analysis, we selected ACTA2 and SOX9 as appropriate protein markers to locate SMC-derived cells on the main axis of phenotypic diversity from SMCs (ACTA2+), via fibromyocytes (ACTA2- SOX9-), to chondromyocytes (SOX9+) (**Fig. 2g**). We also mapped LGALS3 for comparison with important studies in the field[10] and examined *Rgs5* expression by RNAscope in situ hybridization to localize the contractile ACTA2+ cells in the pericyte-like SMC1 cluster, which have not previously been mapped in atherosclerotic lesions. Since SMC2 differed from SMC0 by mainly a dissociation-induced gene signature,[20] which is likely induced during processing, we did not pursue a separate analysis of SMC2 in tissues.

Staining in aortic root sections showed a clear topography of subtype localization within lesions, with ACTA2+ TdT+ SMCs confined to the subendothelial cap region (henceforth cap SMCs) and SOX9+ TdT+ chondromyocytes located in the plaque interior (**Fig. 3a,b**). LGALS3+ TdT+ cells mostly co-expressed SOX9, but some LGALS3+ SOX9- TdT+ cells were also found closer to the plaque surface or in the underlying media. *Rgs5*+ TdT+ cells were found within the fibrous cap but also scattered in arterial media beneath and adjacent to the plaque (**Fig. 3c**). Given their partial location in the cap, we henceforth denote the SMC1 cluster as the SMC1/cap cluster.

Plaque ACTA2+ TdT+ cap SMCs, SOX9+ TdT+ chondromyocytes, and LGALS3+ TdT+ cells were directly counted by confocal microscopy. These data were used to calculate the number of ACTA2- SOX9- fibromyocytes, which is possible because of the minimal overlap between ACTA2 and SOX9 expression. We found that 4 weeks of ApoB-LP lowering enriched the SMC-derived cell population for ACTA2+ SMCs, while the proportions of chondromyocytes, fibromyocytes, and LGALS3+ TdT+ cells were not significantly changed (**Fig. 3d**). TdT+ cells showed no significant alteration in *Rgs5* expression (**Fig. 3e**).

The observed increase in the proportion of ACTA2+ SMCs could be caused either by growth of ACTA2+ SMCs or by loss of ACTA2- fibromyocytes or chondromyocytes. To distinguish between these possibilities, we determined the absolute numbers of ACTA2+ SMCs, ACTA2- SOX9- fibromyocytes, and SOX9+ chondromyocytes in each group. The cell numbers suggested that the shift in phenotypes involved depletion of fibromyocytes and chondromyocytes, but differences were not statistically significant at this stage of plaque regression (**Fig. 3f**).

In a new experiment, we therefore increased the period of ApoB-LP lowering to 12 weeks to accentuate changes in plaques. Lesions were again induced by injection of $PCSK9^{D377Y}$ adeno-associated virus and feeding on a high-fat diet for 16 weeks, and mice were then either continued on the high-fat diet (HF group, n=8) or switched to a low-fat diet plus weekly *Apob* antisense oligonucleotide injections for another 12 weeks (12wLF/ASO group, n=9). Plasma ApoB-LP cholesterol and triglycerides were maintained at low concentrations in the 12wLF/ASO mice during the intervention period, leading to smaller lesions with less lipid accumulation, fibrosis, and necrosis than in HF mice (**Fig. 4a,b** and **Extended Data Fig. 3a**). Macrophage numbers were substantially reduced (**Fig. 4c**), and unlike at the 4-week time point, the total number of SMC-derived TdT+ cells was also significantly reduced (2.1-fold) (**Fig. 4d,e**).

Classification of SMC-derived cell subtypes in ACTA2/SOX9 double-stained aortic root sections revealed an accentuated shift in phenotypes, with a 2.8-fold increase in the proportion of ACTA2+ TdT+ cap SMCs, an unaltered proportion of ACTA2-SOX9- fibromyocytes, and a 1.5-fold decrease in the proportion of SOX9+ chondromyocytes (**Fig. 4e**). Expression of *Rgs5*+ in TdT+ plaque cells was numerically increased consistent with skewing towards contractile cells, but the difference was not significant (**Fig. 4f**). Importantly, the absolute cell counts clearly showed that loss of modulated ACTA2- subtypes — both fibromyocytes and chondromyocytes — was the dominant process underlying the change in the distribution of SMC-derived cell subtypes (**Fig. 4g**). This was substantiated by a complete loss of KI67, a marker of proliferating cells, among ACTA2- SMC-derived cells (**Fig. 4h,i**). Since fibromyocytes and chondromyocytes are abundant subtypes and the main producers of extracellular matrix in plaques, their depletion explains the loss of fibrous tissue and the substantial plaque shrinkage. Notably, the total number of ACTA2+ TdT+ cap SMCs remained stable even after 12 weeks of ApoB-LP lowering.

Endothelium-derived cells are lost in regressing plaque

In both the 4-week and the 12-week regression experiments, we noted a small contribution of ACTA2+ cells derived from TdT- cells, but the number did not differ significantly between groups at either time point (**Extended Data Fig. 3b**). To test whether these cells were derived from endothelial cells through endothelial-to-mesenchymal transitioning, which has been shown to contribute to cap ACTA2+ cells in some contexts,[24] we repeated the 4-week regression experiment in Cdh5-$CreER^{T2}$ x TdT mice with lineage-traced endothelial cells. Endothelial-derived TdT+ cells were observed inside plaques, both in larger strands parallel to the plaque surface, near the bottom of invaginations, and as individual cells (**Extended Data Fig. 4a-d**). Notably, they were significantly decreased in regressing compared with progressing plaque (**Extended Data Fig. 4e**). However, most remained CD31+, and detectable ACTA2 expression was not common and always below the levels of other cap cells, indicating they had not undergone full endothelial-to-mesenchymal transitioning to SMC-like cells.

Consistent set of genes regulated in SMC-derived cells

To analyze the gene regulation underlying fibromyocyte and chondromyocyte depletion, we performed scRNA-seq analysis of pooled aortic arches from each group in the 12-week regression experiment. SMC-derived cells showed highly reproducible clustering into the same subtypes identified in the 4-week regression experiment, and both data sets were analyzed for differentially expressed genes (DEGs) in each SMC-derived cell subtype between the LF/ASO and HF groups (**Fig. 5a-b** and **Extended Figs. 5-6**). Full data on DEGs in each cluster and across the entire cell population at the 4-week and 12-week time points are presented in **Supplementary Tables 2-3**.

To deplete our lists of DEGs for false positives, we focused our analysis on genes significantly regulated at both time points. Fibromyocytes and chondromyocytes had the most conserved gene regulation (75 and 117 genes, respectively) (**Fig. 5c**), and the direction of gene expression changes resulting from ApoB-LP lowering was highly consistent between time points (**Fig. 5d**). Transcripts that were consistently downregulated by ApoB-LP lowering in fibromyocytes and chondromyocytes comprised multiple with described functions in immune defense, including *C3, Lcn*2, *Mmp3*, *Mt1*, *Mt2, Vcam1, Hp,* and *C4b*. Interestingly, many of these genes were among the regulated genes in a pioneering microarray study of whole murine plaques.[25] Transcripts increased by ApoB-LP lowering in fibromyocytes or chondromyocytes included genes with a role in contractile phenotype (*Acta2*, *Mef2a, Lmod1, Tagln, Gucy1a3),* and calcium handling (*Crispld1, Ahnak*). Changes in gene regulation in the other SMC-derived subtypes showed less overlap and directional consistency (**Supplementary Fig. 1**).

The observed differences in fibromyocyte and chondromyocyte gene expression were validated by in situ hybridization in aortic root sections of HF and 4wLF/ASO mice for two of the most regulated genes, *C3* and *Lcn2*. Both transcripts were detected in the modulated TdT+ cells in the plaque interior (**Fig. 6a**), and their expression was substantially reduced by 4 weeks of ApoB-LP lowering (**Fig. 6b**).

To reach very low ApoB-LP levels, the intervention in 4wLF/ASO mice involved a diet change and the blockade of hepatic *Apob* expression. This raised the question of whether the diet change itself, rather than the decrease in ApoB-LPs, could drive the observed gene regulation. To address this issue and extend the findings to another atherosclerosis model and both sexes, we analyzed *C3* expression in plaques of male and female HF-fed *Ldlr* knockout mice with established atherosclerosis that were subjected to 4 weeks of *Apob* ASO treatment (4wHF/ASO) or a control ASO (HF) (**Fig. 6c** and **Extended Data Fig. 7a,b**). This analysis was possible without lineage tracing because *C3* is specifically expressed in SMC-derived cells in murine atherosclerosis (**Extended Data Fig. 7c,d**). We found that *C3* expression was robustly decreased in both sexes by ApoB-LP lowering without diet change (**Fig. 6d**).

Potential upstream regulators of the altered gene expression

We next sought to understand the upstream signaling pathways that trigger the changes in gene expression and the depletion of modulated SMC-derived cells from regressing plaque. The contractile phenotype is maintained by a complex of serum response factor (SRF) and myocardin (MYOCD) that binds CArG boxes in the promoters of contractile genes and stimulates their expression.[26] Previous work identified multiple regulatory mechanisms through which the action of MYOCD/SRF can be reduced, leading to loss of the contractile phenotype and the conversion of SMCs to alternative cell types. These mechanisms include upregulation of KLF4, leading both to reduced *MYOCD* expression and the disruption of MYOCD function;[10,27] NFκB signaling, which disrupts assembly of the SRF/MYOCD/CArG box ternary complex and drives SMC proliferation;[28] and cholesterol overload, which can reduce MYOCD expression and induce inflammatory signaling in SMCs.[29]

To assess the potential importance of NFκB- and KLF4-dependent gene regulation, we performed SCENIC analysis to identify transcription factor-controlled regulons that were differently expressed in the 4wLF/ASO and 12wLF/ASO mouse groups and their respective HF control groups. Among the top differentially expressed regulons were several of the NFκB pathway (Rel, Relb, Nfkb1, Nfkb2) (**Fig. 7a** and **Supplementary Tables 4-5**). NFκB regulons were highly active in fibromyocytes and chondromyocytes in the progressing atherosclerotic lesions in the HF groups, but this type of signaling was almost completely lost after 12 weeks of plaque regression (**Fig. 7b**). No changes in the Klf4 regulon were detected.

To corroborate that NFκB signaling is high in fibromyocytes and chondromyocytes in progressing atherosclerotic lesions, we also reanalyzed scATAC-seq data (single-cell assay for transposase-accessible chromatin) from atherosclerotic mouse aorta deposited by Wang et al.[30] NFκB binding motifs were increased and SRF binding motifs decreased in open chromatin of fibromyocytes and chondromyocytes compared with contractile SMCs, consistent with active canonical NFκB signaling that disrupts MYOCD/SRF signaling (**Fig. 7c**). To test whether this also applies to human atherosclerosis, we reanalyzed snATAC-seq (single-nuclei ATAC-seq) from atherosclerotic human coronary arteries deposited by Turner et al.[31] The cluster of SMC-derived cells was isolated, and cells were annotated using human scRNA-seq data and terminology from Wirka et al., in which modulated SMCs are collectively termed fibromyocytes (no chondromyocyte cluster) (**Fig. 7d**).[12] REL, RELA, and RELB family binding motifs were specifically enriched in this cluster. NFKB1 and NFKB2 motifs were also increased in open chromatin of some cells outside the modulated SMC cluster, but it should be noted that NFKB1 and NFKB2 do not have transcriptional activity and may be inhibitory when not complexed with REL factors.[32] The combination of SCENIC and sn/scATAC analysis thus points to reduced NFκB signaling as a strong regulator of gene expression in modulated SMC-derived cells in regressing plaque.

To evaluate the possibility that lipid depletion from SMC-derived foam cells could be involved, we used the fluorescence of Oil Red O to map neutral lipids in SMC-derived cells. Engorgement of SMCs and SMC-derived cells with cholesteryl esters is a prominent feature of atherosclerosis in mice and humans, but the reversibility of this type of foam cell formation has not been studied. We found that SMC-derived foam cells are significantly reduced by ApoB-LP lowering already after 4 weeks (**Fig. 7e-f**), suggesting that lipid depletion from SMC-derived cells could be a potential factor driving the observed changes in gene expression.

Top DEGs are downstream of NFκB signaling

Finally, to evaluate whether these upstream regulators can explain the observed changes in fibromyocyte and chondromyocyte gene expression, we conducted a series of *in vitro* studies. NFκB signaling is downstream of receptors for the inflammatory cytokines TNF and IL1β, which are expressed on SMC-derived cells (**Extended Data Fig. 8**). Interestingly, cholesteryl ester overload in SMCs has been suggested as an additional intrinsic driver of NFκB signaling,[15,29] but this has to our knowledge not been directly tested. To map genes controlled by NFκB signaling in SMCs and to test whether foam cell formation drives NFκB signaling, we cultured primary aortic murine SMCs in the presence of cyclodextrin-complexed cholesterol, which induces cholesteryl ester accumulation and foam cell formation in SMCs,[33] or the prototypical NFκB activator tumor necrosis factor (TNF), with or without blocking canonical NFκB signaling by knockdown of *Ikbkb* (**Fig. 8a**). Principal component analysis of RNA-seq data revealed great overlap in the regulated genes between foam cell induction and TNF treatment (**Fig. 8b**). It also showed that the bulk of gene expression changes induced by cholesterol loading in SMCs could be blocked by inhibiting canonical NFκB signaling. These findings were replicated in an independent experiment (**Extended Data Fig. 9**). The regulation of selected genes is shown in **Fig. 8c**.

Most importantly, the TNF- and foam cell-induced gene expression phenocopied major portions of the transcriptional changes that occur in fibromyocytes and chondromyocytes in response to ApoB-LP lowering *in vivo*. Both stimuli induced most of the genes downregulated in response to ApoB-LP lowering, including top-regulated genes like *Lcn2, C3, Mmp3, Hp, Vcam1,* and *Cxcl1* (**Fig. 8d**). Conversely, many genes that were upregulated by ApoB-LP

lowering were repressed by TNF and cholesterol loading, including *Acta2, Gdf10, Slc6A6, Gucy1a3,* and *Comp*. Furthermore, the regulation of these genes was counteracted by simultaneous blockade of canonical NFκB signaling.

The combined data indicate that ApoB-LP lowering efficiently dampens the active NFκB signaling in SMC-derived cells that characterizes progressing atherosclerosis. This may be achieved both by the reduction in macrophage-derived inflammatory cytokines, which are known to be reduced in regressing plaque,[3,34] and by reductions in the intracellular cholesterol load. Considering the known role of NFκB signaling in SMC modulation and proliferation, this explains the loss of proliferation and gradual depletion of fibromyocytes and chondromyocytes in regressing plaques, albeit it may not be the only mechanism involved.

DEGs are enriched for causal atherosclerosis genes

On a more general level, the scRNA-seq data from the present set of experiments provides a map of associations between disease activity and gene expression in SMC-derived cells. Because being associated is a criterion for causality, these data sets may be a useful resource for prioritizing candidate genes and gene pathways in SMC-derived cells that could be targeted for atherosclerosis therapy.

To confirm that the lists of differentially expressed genes in different SMC-derived cells are helpful in finding causal genes, we first analyzed whether they are enriched for genes previously shown to affect plaque development in mice. All genes have not been tested for their implication in mouse atherosclerosis; nevertheless, we considered that enrichment for known causal genes would also indicate enrichment for as-yet unknown causal genes. Using data from a meta-analysis of mouse atherosclerosis studies,[35] we found highly significant enrichment of causal genes among DEGs in the fibromyocyte and chondromyocyte clusters (**Fig. 8e**). Overlapping genes are listed in **Supplementary Table 6**.

To analyze whether the lists also contain information that can aid in the identification of human causal genes, we next analyzed if their human homologs are enriched for genes with a genetic association to atherosclerosis. To this end, we used a list of GWAS genes with quasi-significant linkage (1% FDR) to coronary artery disease from a recent large genome-wide association study.[36] Significant enrichment was seen for DEGs in fibromyocytes (**Fig. 8f**), thus identifying the following overlapping genes as candidate targets for modulating the response of SMC-derived cells in atherosclerosis: *CXCL12, GUCY1A3, CD109, SMAD7, CRISPLD1, ITIH4, MYH11, NBEAL1,* and *ASAP2*.

Discussion

ApoB-LP lowering drugs, such as statins, ezetimibe, and PCSK9 inhibitors, partially protect patients with advanced atherosclerosis against disease progression and clinical events, but true plaque regression is difficult to achieve clinically within a short time frame. Even at the lowest ApoB-LP concentrations achieved with drug therapy, the average shrinkage of lesions is small, and there is a considerable residual risk of new clinical events.[37,38]

Recent efforts to stop atherosclerotic disease activity more efficiently have focused on anti-inflammatory drugs. ApoB-LP lowering itself leads to the resolution of inflammation, but the clinical success of anti-IL1β and colchicine indicates that the immune-dampening effect is not always sufficient and that potentiating it improves the standard of care.[7,8] Following a parallel line of reasoning, we postulated that SMC-derived cells might mediate part of the beneficial mechanisms of ApoB-LP lowering and that characterizing the underlying mechanisms could uncover targets for add-on therapies to achieve faster plaque regression. In the present study, we provide the first analysis of the impact of ApoB-LP lowering on SMC-derived cells in a mouse model of atherosclerosis.

The main finding of this study was that ApoB-LP lowering leads to the depletion of SMC-derived fibromyocytes and chondromyocytes, while the size of the cap SMC population remains unaffected. The effect of ApoB-LP lowering on SMC-derived cells has a later onset than on immune cells, but it is likely to have a strong long-term impact on plaque size. Fibromyocytes and chondromyocytes are abundant cell types in plaques and produce the extracellular matrix that constitutes most of the plaque volume. Consistently, the substantial loss of SMC-derived cells after 12 weeks of regression was followed by a marked reduction in collagen-rich tissue and plaque size. Although we used a model drug, *Apob* antisense oligonucleotides, in our experiments, the results will likely extend to other means of ApoB-LP lowering, because no major differences in the pathogenesis of lesions induced by different types of lipoproteins have been detected in mice.

The dissociation between the effects of ApoB-LP lowering on ACTA2+ cap SMCs and the modulated forms of SMC-derived cells is particularly important and follows a series of previous reports of significant differences between contractile and modulated forms of SMC-derived cells. In a dual recombinase-lineage tracing experiment in mice, Alencar et al. found that passage through a *Lgals3*-expressing state is characteristic of most SMC-derived cells except for cap ACTA2+ SMCs.[22] Furthermore, we recently reported that the recruitment of ACTA2+ SMCs into the fibrous cap depends on a Notch-dependent signaling mechanism shared with embryonic arteriogenesis.[39] Blocking this pathway abolished ACTA2+ SMC recruitment without affecting other SMC-derived cells.[39] Cap formation may therefore be a physiological arteriogenic response to recreate a supporting SMC or pericyte-like cell layer for the endothelium that have lost the connection to the arterial media.[40] This makes it different from the accumulation of fibromyocytes and chondromyocytes, which is driven by the ApoB-LP-fueled atherogenic disease mechanism. The distinction has major implications for drug development. Strategies to limit the accumulation of SMC-derived cells in plaques are often stymied by the concern of depleting cap SMCs and thus increase the risk of plaque rupture and clinical events.[41] The data presented here indicate this need not be the case.

The second key finding was that the mechanism for depleting fibromyocytes and chondromyocytes involves reduced NFκB signaling. Previous research showed that NFκB signaling is an important regulator of SMC modulation and proliferation, and part of the molecular mechanism has been delineated.[28] The downstream NFκB effector RelA can physically bind MYOCD through its Rel homology domain and inhibit the assembly of the SRF/MYOCD/CArG box ternary complex, which drives expression of contractile genes in SMCs.[28] Conversely, MYOCD also inhibits downstream transcriptional activity of the NFκB pathway and puts a break on NFκB-induced SMC proliferation.[28] The mutual inhibition of the

MYOCD and NFκB pathways is consistent with the pattern of NFκB regulon activity that we observed here, with suppression in contractile SMCs and high activity in fibromyocytes and chondromyocytes.

The promiscuity of the NFκB signaling pathway makes it difficult to infer the upstream stimulators, which are likely to be multiple and complex and include both macrophage-derived cytokines, such as TNF and IL1β, and intracellular cholesterol load. Already tested drugs, such as anti-IL1β,[7] may thus owe part of their clinical efficacy to reduced NFκB signaling in SMC-derived cells. However, it should be noted that blocking IL-1β alone in advanced murine plaque did not phenocopy regression-induced changes in SMC-derived cells because it also depleted cap SMCs.[42]

Through its capacity to couple a shared upstream pathway with diverse downstream pathways,[43] NFκB signaling equips cells with a range of possible responses to the shared stimuli present in inflamed tissue. Responses differ even between the subtypes of SMC-derived cells. Even though cap SMCs must be exposed to many of the same stimuli as fibromyocytes and chondromyocytes, they showed little evidence of NFκB signaling activation, assessed either by SCENIC regulon analysis in contractile cell clusters or in situ hybridization for the downstream genes *C3* and *Lcn2*. This result, again, stresses the potential for precisely targeted interventions in the SMC-derived cell population.

A third new finding was the reduction of EC-derived intraplaque cells in regressing plaque. Endothelial-to-mesenchymal transitioning with or without physical detachment from the endothelial lining has been implicated in atherogenesis.[44] It has also been proposed as an alternative contributor to cap ACTA2+ cells in some contexts.[24] In the present study, we did not find EC-derived cells expressing ACTA2 at a comparable level to SMC-derived cap cells. Therefore, compensatory recruitment of cap SMCs from endothelium could not explain the stability of the ACTA2+ cap population in regressing plaque.

Finally, the scRNA-seq data of SMC-derived cells in progressing and regressing atherosclerosis may help prioritize candidate genes and gene pathways in SMCs for exploration as drug targets. Alterations in NFκB signaling dominated the gene expression changes, and it is known that inhibiting NFκB signaling in SMC lineage cells in mice inhibits the development of atherosclerotic lesions.[45] Unfortunately, broad inhibition of NFκB signaling in humans is unrealistic due to the wide involvement of NFκB signaling in many essential processes in the body. However, the scRNA-seq data may point to multiple individual genes, both NFκB-controlled and not, that are causal and could potentially be targeted by therapy. In support of this, we found that genes regulated in fibromyocytes and chondromyocytes were enriched for genes with a demonstrated regulatory role in plaque development in mouse models. This was not the case for contractile cells, consistent with the stability of these cells during regression. Importantly, genes altered in fibromyocytes also showed enrichment for GWAS hits linked to human coronary artery disease. Why similar enrichment was not found for genes regulated in chondromyocytes is not clear, but it may be because chondroid metaplasia, featuring the full transformation of SMCs to chondrocyte-like phenotype, is rare in coronary arteries, although it may be observed in other human arterial beds.[46]

It should be noted that SMC-expressed genes may influence atherosclerosis without being regulated at the transcriptional level in advanced plaques. This may explain why some human SMC genes with substantial evidence of affecting human atherosclerosis, such as *KLF4* or *TCF21*, did not make the overlapping list. However, for the human GWAS hits that did overlap, it strengthens their candidacy as potential therapeutic targets in advanced plaques. Some of the overlapping genes have already been scrutinized for their role in SMCs and atherosclerosis, such as *CXCL12*, *MYH11*, and *GUCY1A3*.[47] However, no studies to date have explored the actions in plaque SMC-derived cells of the other overlapping GWAS hits, such as the genes encoding the transmembrane proteins *CD109* and *SMAD7* in atherosclerosis, which are

regulators of TGFβ signaling,[48] CRISPLD1, which may regulate Ca2+, NBEAL1, which is involved in cellular cholesterol sensing,[49] the serine protease ITIH4, or the proposed vesicular transport regulator ASAP2.

Taken together, our results uncover a new pathway by which ApoB-LP lowering leads to the depletion of SMC-derived fibromyocytes and chondromyocytes while retaining the population of stabilizing cap SMCs. We also show that the depletion mechanism involves major changes in NFκB signaling and that the regulated target genes include several with genetic evidence for causal roles in human atherosclerosis. It remains to be seen if the alterations in the distribution of SMC-derived cells observed in regressing murine plaque also occur in regressing human plaque. Additionally, it will be of interest to study the murine model in further detail to uncover more of the underlying signaling mechanisms and design interventions that can expedite plaque regression.

Methods

Animals

Procedures were reviewed by the ethical review boards at CNIC and Universidad Autónoma de Madrid and approved by the Comunidad de Madrid with the license number PROEX 050/16 and PROEX 265/16. Myh11-CreER^{T2} mice (B6.FVB-Tg(Myh11-icre/ERT2)1Soff/J) and Cdh5-CreER^{T2} mice (B6-Tg(Cdh5-cre/ERT2)1Rha)), which express tamoxifen-inducible CreER^{T2} under the SMC-specific *Myh11* promoter and the endothelial-specific *Cdh5* promoter, respectively, were intercrossed with TdTomato (TdT) reporter mice (B6.Cg-*Gt(ROSA)26Sor*$^{tm14(CAG-tdTomato)Hze}$/J), in which active Cre removes a *loxP*-flanked STOP cassette in a transgene encoding the red fluorescent protein TdT. The Myh11-CreER^{T2} and TdTomato strains were from Jackson Laboratory and had been backcrossed extensively (> 10 times) to the B6 strain. The Cdh5-CreER^{T2} mice were created by the Ralf Adams lab and shared with CNIC on a previous occasion. *Ldlr* knockout mice (B6.129S7-*Ldlr*^{tm1Her}/J) were obtained from the Jackson Laboratory and bred at CNIC. Mice were housed in a specific pathogen free environment with a 12-h light–dark cycle at 23° ± 1°C and 50 ± 5% humidity with free access to drinking water. Unless noted otherwise, mice were fed standard laboratory diet (D184, SAFE).

Myh11-CreER^{T2}xTdT male offspring (because the Myh11-CreER^{T2} transgene is integrated in the Y chromosome) were treated at 6 weeks of age with 5 daily intraperitoneal (i.p.) injections of 1 mg tamoxifen (T5648, MilliporeSigma) dissolved in corn oil to activate TdT in SMCs and allow lineage tracing of SMC-derived cells, respectively. Four weeks later, hypercholesterolemia was induced by i.v. injection of rAAV8-mPCSK9^{D377Y} virus particles (1×10^{11} vector genomes per mouse, produced at the CNIC Viral Vector Facility) combined with feeding a high-fat diet (S9167-E011, SNIFF Spezialdiäten GmbH) containing 25% fat with 8.9% coconut oil and 0.8% cholesterol. After 16 weeks of atherosclerotic plaque development, mice in the HF groups were maintained on the high-fat diet for a further 4 weeks (two experiments, n=9 and n=6) or 12 weeks (n=8), whereas mice in the LF/ASO groups were shifted to the standard low-fat laboratory diet plus weekly injections (5 μg/g i.p.) of an antisense locked nuclei acid (LNA) oligonucleotide targeting a sequence in *Apob* mRNA for 4 weeks (4wLF/ASO, two experiments, n=14 and n=7) or 12 weeks (12wLF/ASO group, n=8). The antisense oligonucleotide (Qiagen, cat.no. 339532 with custom sequence 5'-3': +A*+G*+C*A*T*T*G*G*T*A*T*+T*+C*+A*, where + marks LNAs and * phosporothioate bonds) was previously described by Bartels et al.[2] One experiment also included mice shifted to the low-fat diet plus injection of a control antisense oligonucleotide with a scrambled sequence (Qiagen, cat.no. 339532 with sequence 5'-3': A*A*C*A*C*G*T*C*T*A*T*A*C*G*C*; placement of LNAs not revealed by company) (4wLF group, n= 13). The 4-week regression experiment with HF (n=10) and 4wLF (n=11) groups was repeated in male Cdh5-CreER^{T2} mice. *Ldlr-/-* mice were fed the high-fat diet for 24 weeks followed by 4 weeks of either *Apob* antisense oligonucleotides (4wHF/ASO, n=5 males, n=5 females) or the control antisense oligonucleotides (HF, n=5 males and n=4 females).

Serial blood samples were obtained from the submandibular vein throughout the studies. At the endpoint, mice were anesthetized by i.p. injection of pentobarbital (250 mg/kg) and lidocain (20 mg/kg). The thoracic cavity was quickly opened, and blood was drawn from the right ventricle. The mouse was then exsanguinated by cutting the right auricle followed by stopping the heart in diastole by perfusion of a 50mM KCl solution through the left ventricle. For single-cell RNA extraction, the whole aortic arch (including ascending aorta, aortic arch, and part of the descending thoracic aorta) was quickly removed and preserved in cold Hanks' balanced salt solution (HBSS) containing 1% fetal calf serum (FCS). Hearts, including the aortic root, were fixed in 4% phosphate-buffered formaldehyde overnight.

Plasma cholesterol and triglycerides

Plasma cholesterol was measured in duplicate with an enzyme assay (Thermo Fisher Scientific TR13421). Plasma HDL cholesterol was measured after precipitation of ApoB-containing lipoproteins with the Randox HDL-c reagent (Randox CH203). ApoB-LP cholesterol was calculated as total cholesterol – HDL cholesterol. Plasma triglycerides were measured with a kit (Siemens, DF69A) run on a Dimension Bioanalyzer Rxl Max instrument (Siemens).

Immunofluorescence and microscopy

The upper part of the heart, containing the aortic root, was cryoprotected in sucrose solution (25% and 50% in PBS), embedded in OCT (Sakura Tissue-Tek 4583), and snap-frozen. Aortic root cross-sections (5 μm) were collected starting at the level of the commissures of aortic valves.

The following double immunofluorescence stainings were performed: 1) anti-ACTA2 (biotinylated mouse monoclonal, Neomarkers MS-113-BO) and anti-CD68 (rabbit polyclonal anti-CD68, Abcam, ab125212) followed by Streptavidin-Alexa647 (Thermo Fisher Scientific, S21374) and Alexa488–conjugated goat anti-rabbit (Molecular Probes, A11034); 2) anti-ACTA2 and anti-TYROBP (rabbit monoclonal antiDAP12, Abcam, ab283703) followed by Streptavidin-Alexa647 and Alexa488–conjugated goat anti-rabbit; 3) anti-LGALS3 (rat monoclonal, CedarLane Laboratories, CL8942) and anti-SOX9 (rabbit monoclonal, Abcam, ab185230) followed by Alexa 488–conjugated goat anti-rat (Molecular Probes, A11006) and Alexa647-conjugated chicken anti-rabbit (Molecular Probes, A21443); 4) anti-ACTA2 and anti-SOX9 (same antibodies as above) followed by Streptavidin- Alexa488 (Thermo Fisher Scientific, S11223) and Alexa647-conjugated chicken anti-rabbit ; 5) anti-ACTA2 and anti-Ki67 (rabbit monoclonal anti-Ki67, Abcam, ab16667) followed by Streptavidin-Alexa488 and Alexa647-conjugated chicken anti-rabbit; and 6) anti-ACTA2 and anti-CD31 (anti-CD31 hamster monoclonal, Millipore Sigma, MAB1398Z) followed by Streptavidin-Alexa488 and Alexa680-conjugated goat anti Armenian Hamster (Jackson ImmunoResearch, 127-625-160). All primary antibodies were diluted 1/100 or 1/200 and all secondary antibodies to 1/500. Nuclei were stained with Dapi (Sigma-Aldrich 1.24653), and slides were mounted in SlowFade Antifade mounting medium (Invitrogen S36937).

In situ hybridizations were performed using a RNAscope Multiplex Flourescent Reagent Assay kit (ACD, 323100) according to the manufacturer's recommendation except for lower volumes. The following probes were used: ACD Bio 417841-C3 for *C3;* ACD Bio 313971-C2 for *Lcn2*, and ACD Bio 1430181-C1 for *Rgs5*. All probes were visualized with Opal 690 reagent (Akoya Biosciences FP1497001KT). Because TdT fluorescence is lost during processing, we stained SMC-derived cells after in situ hybridization with a rabbit anti-RFP antibody (Abcam, ab62341) followed by Alexa568-conjugated goat anti-rabbit (Thermo Fisher Scientific A11011).

Fluorescence was analyzed with a Nikon A1R scanning confocal system coupled to a Nikon Ti-Eclipse microscope with a Plan Apo VC 20x/0,75 DIC N2 dry objective. The entire aortic root was scanned using tile-scan acquisitions with 405 nm, 488 nm, 562 nm, and 642 nm lasers. Images were acquired with NIS Elements AR4.30.02 software.

Samples were stained with Oil Red O for neutral lipids and Sirius for collagen using standard methods, and slides were scanned with a NanoZoomer 2.0RS (Hamamatsu) digital slide scanner with 20x magnification. Oil Red O-stained sections were also analyzed with a Nikon A1R confocal microscope to colocalize signals for Oil Red O (642 nm) and TdT (562 nm).

All image analysis and quantifications were performed in ImageJ distribution Fiji.[50] Plaque areas were outlined manually, and the signal area positive for Oil Red O or Sirius Red was

measured with the threshold tool. To determine the necrotic core area, the necrotic regions were defined as clear areas in Sirius Red-stained sections. Only areas ≥3000μm2 were considered and their sum constituted the necrotic core area. Cell types were counted using a macro to identify all DAPI-stained nuclei followed by manual classification of markers around or within each nucleus. The TdT area with in situ hybridization signal were measured to quantify gene expression within SMC-derived cells. Plaque areas were averaged from 5 sections per mouse; other data types represent 1-2 sections per mouse.

Single-cell RNA sequencing

Aortic arches from the 4wLF/ASO (n=7) and HF (n=6) mouse groups in the 4-week regression experiment and from the 12wLF/ASO (n=9) and HF (n=8) mouse groups in the 12-week regression experiment were cleaned of perivascular tissue and pretreated with 2 mg/ml collagenase II (Worthington LS004174) in HBSS for 15 min at 37ºC to aid adventitia removal. Arches from each group were then washed in HBSS, opened longitudinally, and cut into small pieces. The pieces were incubated for 60 minutes at 37ºC in 3 ml of an enzyme solution containing 200 μg/ml hyaluronidase (Sigma-Aldrich, H3506), 250 μg/ml liberase (Roche, 291963), and 200 μg/ml DNase (Sigma-Aldrich, DN25). Non-digested tissue was disaggregated using a cut Pasteur pipette with rounded edges. Reactions were stopped by adding PBS containing 0.5% bovine serum albumin (BSA). The suspension was passed through a 70 μm pore filter to remove aggregates. Cells were collected by centrifugation (350 g) and resuspended in 300 μl PBS+0.5%BSA. DAPI (1 μg/ml final concentration) and Draq5 (Thermo Scientific 65-0880-96; final concentration, 5 μM) were added, and viable cells (Draq5 positive and DAPI negative) were sorted with a FACSAria Cell Sorter.

Sorted cells were recounted and their viability checked on a Countess III cell counter (Thermofisher). Up to 16500 cells were loaded into each port of a Chromium Next GEM Chip G (10x Genomics). After reverse transcription and cDNA amplification, sequencing libraries were prepared using the Chromium Next GEM Single Cell 3' Kit v3.1 (10x Genomics). Mean library size was calculated using a 2100 Bioanalyzer (Agilent), and the concentration was determined with a Qubit® fluorometer (Thermofisher). Libraries were sequenced in paired-end reads using a HiSeq 4000 system (Illumina) and processed with RTA v1.18.66.3. FASTQ files for each sample were obtained using the cellranger demux pipeline (10x Genomics).

Single-cell bioinformatics

The single-cell transcriptome profile was obtained using the 10X CellRanger pipeline (v3.1.0) and the mouse mm10 genome reference (Ensembl gene build v84) with the TdT transgenic mRNA sequence added.

Single-cell filtering and clustering were done with the Scater[51] and Seurat[52] packages in R (v4.1.2). Cells were filtered as follows: '1000 < UMIs < 35000', 'genes detected > 800', 'percent MT UMIs < 15%', 'Cell UMIs / Total > 0.4%', reads among top 50 genes <65%. Doublets were identified using DoubletDetection (v2.4)[19] and were removed from the analysis, yielding a total of 5605 and 4794 cells for the 4wLF/ASO and HF samples in the 4-week regression experiment and 4383 and 4169 cells for the 12wLF/ASO and HF samples in the 12-week regression experiment. Cells were log-normalized and scaled. Clustering and dimensionality reduction of all cells were done using Seurat R methodology with the most variable genes selected by the mvp method with 1 > mean > 100 and 0.15 > dispersion > 4 cutoffs, yielding 526 and 510 genes for the 4- and 12-week experiment, respectively, 20 principal components, and 0.25 resolution distance. SMC-derived cells were selected based on clusters expressing the TdT transgene and re-clustered using most variable genes selected by the mvp method with 1 > mean > 100 and 0.25 > dispersion > 4 cutoffs, yielding 267 and 371

genes for the 4- and 12-week experiment, respectively, 20 principal components, and 0.34 resolution distance. Top cluster markers and genes differentially expressed between conditions were identified with the MAST method and Bonferroni-adjusted p values, with testing restricted to genes detected in at least 30% for marker detection and 10% for differential expression between conditions in cells in any cluster. Transcripts *Gm42418* and *AY036118* were removed from the analysis because they correspond to 18S RNA (*Rns45s*). Natural logarithm (log) fold changes are reported. Datasets were integrated with samples from public datasets (GSE150644, GSE131776) from the NCBI Gene Expression Omnibus using reciprocal principal component analysis to compare SMC-derived cellular diversity.
Regulon activity analysis was performed using the SCENIC[23] pipeline with default parameterization. For comparison between clusters, we considered only those regulons active in more than 50% of the cells in at least one cluster. For comparison between conditions within each cluster, we considered only those regulons detected in at least 10% of cells in any condition, and significant differences in the activity of regulons were detected by two-sided Yates' continuity corrected Chi-square test and adjusted for false discovery rate by the Benjamini–Hochberg method.

Re-analysis of chromatin accessibility data

We re-analyzed publicly available data of transposase-accessible chromatin of single cells or nuclei using sequencing (sc/snATAC-seq) of atherosclerotic mouse aorta (PRJNA716327) and human coronary artery (PRJNA733106).[30,31] Datasets were collected from the NCBI Sequence Read Archive and processed using Cell Ranger ATAC v2.1.0 with either mouse (mm10) or human (GRCh38) 10X reference genome (build 2020-A). The mouse aorta single-cell dataset was analyzed using a modified workflow in Signac v1.10.[53] We rescued only the barcodes with a minimum of 2000 fragments detected, more than 10% of fragments located in peaks, and transcription start site enrichment above 2. Single-cell RNA-seq data of HF samples (12-week experiment) was used as a reference to map cell annotations and UMAP structure to the mouse ATAC-seq dataset. The human coronary single-nuclei dataset was re-analyzed with ArchR v1.0.2 according to a workflow in the original publication of the dataset.[31,54] Single-cell RNA-seq data and cluster names from Wirka et al. (gene expression omnibus accession code GSE131780) were used for human cell annotation.[12] DNA motifs recognized by NFκB family transcription factors were retrieved from the JASPAR2020 database,[55] and motif accessibility deviation was estimated with the chromVAR algorithm implemented in Signac.[56]

Enrichment for mouse causal genes and human GWAS hits

For enrichment analysis, lists of DEGs in each cluster that were significantly regulated in the same direction at 4 and 12 weeks of regression, and lists of non-DEGs, restricted to genes expressed in at least 1% of SMC-derived cells with at least 3 UMI counts per cell, were compared for overlap with a list of 827 mouse genes with proven causal involvement in mouse atherosclerosis[35] or with a list of mouse homologs of human genes located near SNPs associated with coronary artery disease at a false-discovery rate of 1% in a large genome-wide association study.[36] To translate between mouse and human genes, we used Ensembl archive 105 (December 2021). The GWAS hits were translated to Ensembl IDs (hg37) and then those, in turn, were translated to mouse Ensembl IDs and genes using the biomaRt R package. Mouse scRNA-seq-derived genes (mm10, Ensembl 80 from May 2015) and the list of mouse causal genes were updated according to the same Ensembl archive version as for human genes. 2x2 tables were constructed with the number of DEGs and non-DEGs in columns and the number of overlapping and non-overlapping genes in rows, and significant increases in overlapping

were detected by one-sided exact Fisher test. Calculations were performed in R (v4.2.3), and graphics were plotted using the ggplot2 R package.

Primary mouse SMC experiments

To establish cultures of primary aortic SMCs, C57BL/6JRj male mice (6 weeks old, Janvier Labs) were euthanized, and the heart was perfused through the apex with sterile HBSS. Aortas (a pool of 15 per experiment) were dissected and the perivascular tissue removed, followed by two washes in ice-cold HBSS. To facilitate removal of the adventitial layer, aortas were placed in 2 mg/ml collagenase II enzyme solution for 10 min at 37°C followed by washing in DMEM/F12 media. The adventitia was stripped off, and the aortas were opened longitudinally and washed in DMEM/F12 to remove blood clots. The endothelial layer was then removed by gently scraping with fine forceps followed by washing in DMEM/F12 and mincing of the remaining medial layer into small pieces with scissors, which were incubated with an enzyme solution (2 mg/ml collagenase II, 1 mg/ml soybean trypsin inhibitor, 0.75 U/ml elastase, 1% penicillin/streptomycin in HBSS) for 1 h at 37°C with shaking. The digested aorta tissue was then pipetted up and down several times, and the cell suspension was filtered through a 70-μm cell strainer before undergoing 3 cycles of centrifugation (200g, 5 min, room temperature) and washing in DMEM/F12 to remove the enzyme solution. The cell pellet was finally resuspended in DMEM/F12 containing 20% FCS and 1% penicillin/streptomycin, and cells were seeded into collagen type I-coated 24-well culture plates. Two days later, the medium was changed to DMEM/F12 containing 10% FCS and 1% penicillin/streptomycin. For induction experiments, aortic SMCs at ~80% confluency (P4) were serum-starved for 24 h.

We performed two different experiments with gene expression profiling by RNA-sequencing. In experiment A, control (transfected with 10 μM control siRNA) and *Ikbkb*-deficient cells (transfected with 10 μM *Ikbkb* siRNA) were left untreated or exposed to water-soluble cholesterol (Sigma-Aldrich, C4951, final concentration 10 μg/ml) for 72 hours. In experiment B, control and *Ikbkb*-deficient cells were left untreated or exposed to human TNF (ab259410, final concentration 10 ng/ml in PBS containing 0.1% BSA) for 24 hours. Transfection of siRNAs in mouse aortic SMCs was carried out using Opti-MEM (Thermo Fisher) and Lipofectamine RNAiMAX (Invitrogen) for 18 h on two consecutive days. To knockdown *Ikbkb*, we used a pool of two independent mouse siRNAs with the following target sequences: CAGGTTATCATAGGCAGGTAT and CTGCTGTTTCTGGTCCTTTAA (Qiagen FlexiTube siRNA, cat. no SI05163242, SI01075235). As control siRNA we used the AllStars negative control siRNA (Qiagen, cat. no. 1027280). For each condition, we obtained RNA from 4 independent replicates for RNA sequencing (each consisting of 3 pooled wells) using the NucleoSpin RNA Plus Kit (Macherey-Nagel, 790984).

We conducted an independent validation experiment in the same way with 3 independent replicates per condition and analyzed the expression of selected genes by quantitative real-time PCR as described below.

RNA sequencing

RNA was isolated and was sequenced by BGI (Copenhagen, Denmark). All RNA samples passed quality control (Agilent 4200 electrophoresis system). Non-stranded DNA libraries were prepared with polyA-selected mRNA, and 100 bp paired-end sequencing was conducted with at least 20M pair reads per sample using DNBSEQ. RNA sequencing data were processed with the Nextflow-based pipeline "nf-core/rnaseq" (v3.9).[57] Sequenced reads were aligned to the GRCm38 mouse reference genome using STAR aligner (v2.6.1d), and gene-level quantification was done with Salmon (v1.5.2). The reference genome sequence and gene annotation were downloaded from AWS iGenome (https://github.com/ewels/AWS-iGenomes)

using the Ensembl version as a source. Further analysis was performed in R (v4.2.3) with Bioconductor (v3.14) packages. Gene counts were imported using tximport.[58] Gene filtering was performed as previously described,[59] and only genes with ≥10 counts per million (CPM) in at least 3 samples were analyzed. DESeq2 was used for data normalization, principal component analysis after variance stabilizing transformation, and estimation of differential gene expression between compared groups. Results with p values adjusted for false discovery rate (p_{adj}) <0.05 were considered statistically significant. Log2-fold changes are reported.

Quantitative real-time PCR analysis

Complementary DNA synthesis was performed using 0.5 μg RNA with the RevertAid First Strand cDNA synthesis kit (Thermo Scientific). For Quantitative real-time PCR, 100 ng cDNA served as the template for PCR amplification using the Maxima SYBR® Green QPCR Master Mix (Thermo Scientific) in an Aria Mx3000P qPCR System (Agilent Technologies, Santa Clara, CA). Each reaction was run in duplicate, and relative gene expression levels were normalized to mouse hypoxanthine-guanine phosphoribosyltransferase (*Hprt1*). Relative expression was calculated using the ΔΔCt method. The following primers for mouse genes were used:

Oligo Name	Sequence (5'->3')
m_Lcn2_F	acggactacaaccagttcgc
m_Lcn2_R	agctccttggttcttccatacag
m_Il6_F	acaagtccggagaggagactt
m_Il6_R	agaattgccattgcacaactcttt
m_Vcam1_F	gtccgttctgaccatggagc
m_Vcam1_R	ggatccttggggaaagagtagatg
m_C3_F	tatgggaccagcttcagggt
m_C3_R	tgggagtaatgatggaatacatggg
m_Hprt1_F	cccagcgtcgtgattagcg
m_Hprt1_R	cacttttccaaatcctcggcat

Statistics and reproducibility

Bars in dot blots represent mean ± SEM for normally distributed data and median and interquartile range for non-normally distributed data, as indicated in the figure legends. For data with normal distribution, p values were calculated by two-sided unpaired Student t-test (with Welch's correction in case of difference in group variance), one-way or repeated-measures ANOVA with Tukey's or Šidák post-test, or a mixed-effects analysis with Šidák post-test. For other data distributions, two-sided Mann-Whitney test or Kruskal-Wallis test followed by Dunn's post-test was used. The calculations were performed in Prism 9 (GraphPad Software), and differences were considered statistically significant at $p < 0.05$. Statistical analysis of single-cell and bulk RNA-seq data, SCENIC regulons, and enrichment for causal atherosclerosis genes are described above. Missing data points in analyses are specified in figure legends and were always explained by random technical issues, e.g. folded or detached cryosections or inadequate plasma sample volume. Micrographs shown in figures are representative examples of staining performed in all mice for which quantified data is reported in the accompanying graphs.

Data availability

Raw and processed scRNA and RNA sequencing data generated in this study has been deposited in BioStudies (ArrayExpress) with the accession numbers E-MTAB-12019 and E-MTAB-13416, respectively. The deposited scRNA-data for SMC-derived cells can be loaded and explored interactively through the Single Cell Data Visualisation Platform (scDAVIS at https://bioinfo.cnic.es/scdavis/ with search input E-MTAB-12019). All other data supporting the findings in this study are included in the main article and associated source files.

We have used raw data deposited at NCBI SRA from published studies PRJNA716327 (SRA accession code SRP311911) and PRJNA733106 (SRA accession code SRP321576), preprocessed data from the Gene Expression Omnibus (accession codes GSE131780, GSE150644, and GSE131776), and the reference genome assemblies mm10 (Ensembl gene build 84, 10X reference build 2020-A based on GENCODE vM23/Ensembl 98), GRCm38 (AWS iGenomes Ensembl reference build), and GRCh38 (10X reference build 2020-A based on GENCODE v32/Ensembl 98).

Code availability

The code used for the enrichment analysis of DEGs for lists of mouse genes and human homologs is available at https://zenodo.org/doi/10.5281/zenodo.10145655

Acknowledgments

We thank members of the CNIC Viral Vectors Unit, Microscopy Unit, Genomics Unit, Bioinformatics Unit, Cellomics Unit, and Animal Facility for excellent technical help, and Simon Bartlett, CNIC, for English editing. This study was supported by grants from the European Research Council (ERC) under the European Union's Horizon 2020 research and innovation programme (grant agreement No 866240, JFB), the Novo Nordisk Foundation (NNF17OC0030688, JFB), the Ministerio de Ciencia e Innovación with cofunding from the European Regional Development Fund (PID2019-108568RB-I00, JFB), the Ministerio de Ciencia e Innovación (BES-2016-076633, PN, and IJC2020-044971-I, DMC), and Aarhus University Research Foundation (Starting Grant, AUFF-E-201 9-723, JAJ). Microscopy was conducted at the Microscopy & Dynamic Imaging Unit, CNIC. CNIC is supported by the Instituto de Salud Carlos III (ISCIII), the Ministerio de Ciencia e Innovación (MCIN) and the Pro CNIC Foundation), and is a Severo Ochoa Center of Excellence (grant CEX2020-001041-S funded by MICIN/AEI/10.13039/501100011033). The funders had no role in study design, data collection and analysis, decision to publish, or preparation of the manuscript.

Author contributions

LC, JAJ, and JFB designed experiments; LC, EHS, VC, DMC, and PN performed animal experiments and analysis of plaques; JAJ performed in vitro experiments; LC, DMC, AB, and AD generated scRNA-seq data; CT, DS, and FSC performed scRNAseq bioinformatics analysis; AM performed scATAC and RNA-seq analysis; DS, PLM, and JFB performed enrichment analysis; VLC designed image analysis tools; LC, JAJ, and JFB interpreted the data and drafted the manuscript with important contributions from AM, DS, CT, DMC, AB, AD, FSC, PN. All authors assisted with manuscript revisions.

Competing interests

The authors report no conflicts of interest.

Figure legends

Figure 1. Effects of 4 weeks of ApoB-LP lowering on plaque morphology and inflammation. a, After induction of atherosclerotic lesions, mice were either maintained on a high-fat diet (HF group), switched to a low-fat diet (4wLF group), or switched to the low-fat diet plus weekly injections of *Apob* antisense-oligonucleotides (4wLF/ASO group). ApoB-LP cholesterol values during the intervention period differed significantly among the three groups. **b**, Quantification of total plaque size, plaque neutral lipid/cholesteryl ester content (stained with Oil Red O), plaque collagen (stained with Sirius Red), and necrotic core area. Representative staining examples are shown in **Extended Data Fig. 1b**. **c,** Representative examples of aortic root sections stained for the macrophage marker CD68. The red channel shows the endogenous TdT signal in SMC-derived cells. The indicated areas (dashed boxes) are shown at higher magnification. **d,** Representative staining for the macrophage marker TYROBP in the same regions. **e-g,** Cell number quantification in the treatment groups, showing decreased absolute and relative CD68+TdT- and TYROBP+TdT- cell numbers in plaques of 4wLF and 4wLF/ASO mice. The absolute number of TdT+ plaque cells was not significantly altered by 4 weeks of ApoB-LP lowering, although there was a non-significant trend to increased relative content consistent with the loss of macrophages. Data are presented as mean±SEM for all mice (n=9/13/14 for HF, 4wLF, and 4wLF/ASO mice, respectively), except in **e** where one data point was missing in the 4wLF/ASO group (due to technical issues), and **f** where the analysis was performed in a subset of mice (n=6/5/12 for HF, 4wLF, and 4wLF/ASO mice, respectively). P values were calculated by repeated-measures ANOVA for the intervention period with Tukey's post-test (**a**) or ANOVA with Tukey's post-test (other panels). L, Lumen. P, plaque. M, media. Scale bars, 200 μm.

Figure 2. Phenotypic diversity of SMC-derived cells shown by scRNA-seq. a-c, Clustering into SMC-derived cells, endothelial cells, and macrophages. The large population of SMC-derived cells is identified by TdT expression. Detection of TdT transcripts in other clusters coincide with cell doublets. **d,** Re-clustering of SMC-derived cells into 5 subclusters. **e**. Marker genes for the 5 subclusters. Genes were selected from among the top 40 genes (including the top 6) showing differential regulation between each cluster and the others. **f.** SCENIC analysis of active regulons (transcription factor-controlled gene sets) in the 5 subclusters. The heatmap shows regulons for which ≥50% of the cells were active in ≥1 cluster. **g.** The expression of genes selected as markers of SMC-derived cell subtypes.

Figure 3. Effects of 4 weeks of ApoB-LP lowering on SMC-derived cell subtypes. a-c, Representative examples of aortic root sections from HF and 4wLF/ASO mice immunostained for ACTA2/CD68 (**a**) and LGALS3/SOX9 (**b**) and in situ hybridized for *Rgs5* mRNA (**c**). Boxed regions are shown at higher magnification in adjacent images. ACTA2+ TdT+ SMCs (white arrows in **a**) reside in the cap region of plaques. Oil Red O staining in an adjacent section shows the significant lipid depletion in the same area after ApoB-LP lowering. SOX9+ TdT+ chondromyocytes (blue arrows in **b**) primarily reside in the plaque interior. LGALS3 is abundant in macrophages (yellow arrows in **b**) but is also expressed in some TdT+ cells, including SOX9+ TdT+ cells. *Rgs5*-expressing TdT+ cells are found in the cap and media (green arrows in **c**). **d,** The percentage of ACTA2+ cap SMCs among all SMC-derived cells is significantly higher in 4wLF/ASO mice than in HF mice. The analysis was performed on all HF (n=9), 4wLF (n=13), and 4wLF/ASO (n=14) mice, but a few data points are missing (1 in the cap SMC/chondromyocyte and 2 in the fibromyocyte analysis) due to technical issues. **e,** Relative content of *Rgs5*+ SMCs among all SMC-derived cells, estimated as the percentage of TdT+ area with colocalized *Rgs5* RNAscope signal. Analyzed in n=6 HF and n=6 4wLF/ASO mice. No significant difference was detected. **f,** Quantification of the absolute numbers of

SMC-derived subtypes among groups. Loss of fibromyocytes and chondrocytes contributes numerically to the increased percentage of SMCs, but differences are not statistically significant. Number of observations as in **d**. Data are presented as median and interquartile range (C, D) or mean±SEM (E, F). P value was calculated by Kruskal-Wallis test followed by Dunn's post-test. L, Lumen. P, plaque. M, media. Scale bars, 200 μm (solid), 100 μm (dashed).

Figure 4. Effects of 12 weeks of ApoB-LP lowering on SMC-derived cell subtypes. a, Plasma ApoB-LP cholesterol concentration was strongly reduced in 12wLF/ASO mice during the intervention period. **b-c,** Total plaque size, plaque neutral lipids (Oil Red O), plaque collagen (Sirius Red), necrotic core area, and the number of CD68+ TdT- macrophages. **d,** Representative examples of ACTA2/SOX9-stained aortic root sections from HF and 12wLF/ASO mice. Some ACTA2+ SMCs (green arrows), SOX9+ chondromyocytes (white arrows), and ACTA2-SOX9-TdT+ fibromyocytes (pink arrows) are marked. **e**. Quantification of total TdT+ cells and their phenotypes. The phenotype distribution is skewed after 12 weeks of ApoB-LP lowering, with a significantly higher proportion of ACTA2+ cells and a significantly lower proportion of SOX9+ cells. **f,** *Rgs5* expression (percentage of TdT+ area) shows a numerical, but not significant increase. **g** The decrease in TdT+ cells and the skewed phenotype distribution is explained by depletion of fibromyocytes (ACTA2- SOX9- TdT+) and chondromyocytes (Sox9+ TdT+), while the absolute number of cap SMCs (ACTA2+) is maintained. **h** Representative examples of KI67-stained aortic root sections from HF and 12wLF/ASO mice. Arrows mark an ACTA2-TdT+ cell (blue arrow) and endothelial cells (white arrows) with nuclear KI67 expression. **i,** Quantification shows significant loss of KI67 expression in ACTA2- SMC-derived (TdT+) cells after ApoB-LP lowering. Data are presented as median and interquartile range (C, J) or mean±SEM (other panels). Analyses were performed in all experimental mice (n=8 HF and n=9 12wLF/ASO mice), but a data point is missing in the HF group in **e,f** and in the 12wLF/ASO group in **b,e,f** (due to technical issues). P values were calculated by repeated-measures ANOVA for the intervention period (**a**), two-sided unpaired t-tests (**b, e-f, h**), in some cases with Welch's correction (**b**), or two-sided Mann-Whitney tests (**c, j**). L, Lumen. P, plaque. M, media. Scale bars, 100 μm (solid), 50 μm (dashed).

Figure 5. Consistent gene expression changes in fibromyocytes and chondromyocytes during plaque regression. a-b. Analysis of differentially expressed genes (DEGs) in scRNA-seq data from the 4-week and 12-week regression experiments. The clustering in SMC subtypes is highly consistent between the two independent experiments (a), but groups show more segregation at the 12-week time point (b). **c-d**. Comparison of significantly regulated genes in each SMC-derived subtype in the two regression experiments. Gene regulation in fibromyocytes and chondromyocytes (C1 and C2) shows substantial consistency in gene expression changes, as shown by the overlap of significant DEGs (c) and the similar direction of DEG regulation after 4 and 12 weeks of ApoB-LP lowering (d). Genes belonging to the top-20 regulated genes in both experiments are colored (up green, down red). Other selected genes are named (black).

Figure 6. Validation of the regulation of top-regulated genes. a, Representative examples of RNAscope in situ hybridization of the two top regulated genes, *C3* and *Lcn2*. Both transcripts were abundant in HF mice in SMC-derived (TdT+) plaque cells and the underlying media. *C3* was also present in the adventitia and perivascular tissue of HF mice. The transcript levels were substantially reduced in regressing plaques and the underlying media of 4wLF/ASO mice. **b,** Quantification of signal in plaque and media. The analysis was performed in all HF (n=9) and 4wLF/ASO (n=14) mice, but a data point is missing for *Lcn2* in situ hybridization (due to technical issues). **c,** Representative examples of *C3* in situ hybridizations

from two groups of HF-fed *Ldlr*-/- mice, one treated with 4 weeks of *Apob* antisense oligonucleotides (4wHF/ASO) and the other with a control oligonucleotide (HF). **d,** *C3* transcription levels were reduced in regressing plaques without changes in overall plaque size. The analysis was performed in n=5/4 female/male HF mice and n=5/5 female/male 4wHF/ASO mice. No differences between males and females were observed. Data are presented as median and interquartile range. P values were calculated by two-sided Mann-Whitney tests. L, Lumen. P, plaque. M, media. A, Adventitia. Scale bars, 200 μm (solid), 100 μm (dashed).

Figure 7. Potential mechanisms governing the shifts in SMC-derived gene expression and phenotype. a, SCENIC analysis of the scRNA-seq data from the 4-week and 12-week experiments, showing differentially expressed regulons (DERs) in fibromyocytes (C1) and chondromyocytes (C2). NFκB regulons (Relb, Nfkb2, and Nfkb1) are prominently regulated at both time points. The analysis considered high confidence regulons that were detected in ≥10% of cells in at least one condition. Adjusted p values were calculated by two-sided Yates' continuity corrected Chi-square test followed by the Benjamini–Hochberg procedure. **b,** Plots of NFκB regulon activity in cells from the 12-week regression experiment split by group, showing that NFκB is induced when SMCs modulate to the fibromyocyte and chondromyocyte phenotypes during high-fat feeding, but that this induction is substantially reversed in these cell subtypes upon ApoB-LP lowering. **c,** Analysis of NFκB and SRF binding motifs in open chromatin of SMC-derived cell subtypes in scATAC-seq data from Wang et al.[30] Cell annotations and UMAP structure were transferred from the scRNA-seq data in our 12-week experiment. **d,** Analysis of NFκB binding and SRF binding motifs in open chromatin of SMC-related subtypes in human snATAC-seq data of atherosclerotic coronary arteries from Turner et al.[31] Cell annotations were transferred from Wirka et al.[12] **e-f,** ApoB-LP lowering leads to lipid depletion in SMC-derived cells. The area of Oil Red O-stained material within TdT+ cells is reduced after 4 and 12 weeks of ApoB-LP lowering compared with matched HF control groups. Plotted data are presented as mean±SEM of n=9 HF, n=13 4wLF, and n=13 4wLF/ASO from the 4-week regression experiment and n=8 HF and n=8 12wLF/ASO from the 12-week regression experiment (one data point missing in LF/ASO groups due to technical issues). P values were calculated by ANOVA followed by Tukey post-test (4w experiment) and two-sided unpaired t-test (12-week experiment). Scale bar, 100 μm.

Figure 8. Differentially expressed genes are controlled by NFκB signaling and enriched for causal mouse and human atherosclerosis genes. a. RNAseq analysis of primary aortic SMCs treated with TNF and cholesterol (chol) loading in combination with *Ikbkb* knockdown (kd) or control siRNA to investigate the involvement of canonical NFκB signaling (n=4 samples per condition). **b.** Principal component analysis. Effects of TNF and cholesterol loading overlap. *Ikbkb* knockdown blocked much of the effect of cholesterol loading, showing the dependency on NFκB signaling. The effect of TNF was not fully blocked consistent with known non-NFκB-mediated effects. **c.** Heatmap of the expression of selected genes, including *C3*, *Lcn2*, known NFκB target genes, contractile genes, and cholesterol-regulated genes. **d.** Integrated analysis, showing that top-regulated genes in fibromyocytes and chondromyocytes in the 4-week (x axis) and 12-week (y axis) regression experiments are regulated by NFκB signaling, irrespective of whether the NFkB signaling is induced by TNF or cholesterol loading. The color coding of the dots shows the direction of gene regulation by TNF/cholesterol overload and the border thickness indicates the dependency on *Ikbkb* in primary SMCs. **e.** Enrichment analysis for mouse atherosclerosis causal genes from the meta-analysis of von Scheidt et al.[35] among the genes consistently regulated at 4 and 12 weeks of plaque regression. Significant enrichment is found for fibromyocytes (C1), and chondromyocytes (C2). **f.** Enrichment analysis for human genes linked to coronary artery disease from Aragam et al.[36]

among the genes consistently regulated at 4 and 12 weeks of plaque regression. Significant enrichment is seen for fibromyocytes (C1). One-sided Fishers exact's tests with Bonferroni-corrected significance level. Percentages indicate the fraction of regulated genes in clusters that overlap with the murine and human lists.

Extended data Figure legends

Extended Data Fig. 1. Additional data for the 4-week regression experiment. a, Plasma total and HDL cholesterol concentrations were measured in serial blood samples during the study. Plasma triglyceride concentrations were measured at the endpoint. **b,** Representative examples of aortic root sections stained with Oil Red O for neutral lipids (mainly cholesteryl esters) and Sirius Red for collagen-rich tissue. Data are presented as mean±SEM for n=9 HF, n=13 4wLF, and n=14 4wLF/ASO mice. P values were calculated with repeated-measures ANOVA for the intervention period with Tukey's post-test (Total and HDL cholesterol) or ANOVA with Tukey's post-test (Triglycerides). Scale bars, 200 μm.

Extended Data Fig. 2. Cluster identification and comparison to public scRNA-seq data. a, UMAP visualization of cell clusters in our scRNA-seq data from plaques and adjacent media. **b-e,** Expression of *Cdh5, Cd68, Tyrobp*, and *Myh11* to identify endothelial cells (*Cdh5*+), macrophages (*Cd68*+ and *Tyrobp*+), and contractile SMCs (*Myh11*+). **f,** Comparison of SMC-derived cells in our data set with other published data sets. SMC-derived cells were isolated and integrated with similar data from Alencar et al.[22] and Wirka et al.[12] by reciprocal principal component analysis. There is high consistency in the detected subgroups of SMCs and SMC-derived cells. Cells were obtained from plaque alone or combined plaque and media in the aortic arch, ascending aorta including the aortic root, or brachiocephalic artery (BCA) of *Apoe* knockout (*Apoe*$^{-/-}$) or rAAV-PCSK9-induced mice as indicated in the labels.

Extended Data Fig. 3. Plasma lipids in the 12-week regression study and TdT-negative cap SMCs. a, Plasma total and HDL cholesterol concentrations were measured in serial blood samples during the study. Plasma triglyceride concentrations were measured at the endpoint. Data are presented as mean±SEM for n=8 HF and n=9 12wLF/ASO mice. P values were calculated with repeated-measures ANOVA for the intervention period with Tukey's post-test (Total and HDL cholesterol) or two-sided unpaired t-test with Welch's correction (Triglycerides). **b,** Counts of TdT-negative ACTA2+ cells in aortic root sections from the 4-week and 12-week regression experiments. Data are presented as mean±SEM for n=9 HF, n=13 4wLF, and n=13 4wLF/ASO mice from the 4-week regression experiment, and n=7 HF and n=8 12wLF/ASO mice from the 12-week regression experiment (missing data points due to technical issues). Differences are not statistically significant.

Extended Data Fig. 4. Endothelial-derived intraplaque cells are reduced in regressing plaque. a, Lineage-tracing of endothelial cells in Cdh5-CreER^{T2} mice subjected to 4 weeks of plaque regression (4wLF/ASO group) or maintained on HF diet (HF group). Endothelial cell-derived cells are observed within plaques (not part of the endothelial lining, examples marked by arrows). The analysis excluded cells that were part of the coronary artery orifices (marked by *). The image is a representative example from the HF group. **b-d,** Endothelial-derived cells were both observed as layers parallel to the surface (**b**), at the bottom of invaginations (**c**), and as isolated cells (**d**). Detectable ACTA2 at the level of other cap cells was rare. Representative examples from the HF group are shown. **e,** Total and CD31+ TdT+ cells, but not the small population of CD31- TdT+ cells, were significantly reduced in regressing plaque. Data are presented as median and interquartile range of n=10 HF and n=11 4wLF/ASO mice. P values were calculated by two-sided Mann-Whitney tests. L, Lumen. P, plaque. M, media. Scale bars, 200 μm (solid), 100 μm (dashed).

Extended Data Fig. 5. Gene expression changes in SMC-derived cells after 4 weeks of plaque regression. Differentially expressed genes (DEGs) were analyzed in SMC-derived cell clusters (C0-C4). Volcano plots show DEGs in each cluster. The top 10 downregulated and upregulated genes after 4 weeks of ApoB-LP lowering are shown in cyan and ochre, respectively. Analysis was performed using the MAST method in Seurat with P values adjusted for multiple testing by the Bonferroni method. The graphs are visual representations of the data in Supplementary Table 2.

Extended Data Fig. 6. Gene expression changes in SMC-derived cells after 12 weeks of plaque regression. Differentially expressed genes (DEGs) were analyzed in SMC-derived cell clusters (C0-C4). Volcano plots show DEGs in each cluster. The top 10 downregulated and upregulated genes upon 12 weeks of ApoB-LP lowering are shown in cyan and ochre, respectively. Analysis was performed using the MAST method in Seurat with P values adjusted for multiple testing by the Bonferroni method. The graphs are visual representations of the data in Supplementary Table 3.

Extended Data Fig. 7. Validation experiment without diet change. a, Experimental design. Male and female *Ldlr*-/- mice were maintained on high-fat (HF) diet and treated for 4 weeks with either *Apob* antisense oligonucleotide (4wHF/ASO group) or a control ASO (HF group). **b,** Measurements of the concentration of total, ApoB-LP, and HDL cholesterol in plasma in each group. Data are presented as mean±SEM for n=4 HF females, n=5 HF males, n=5 4wHF/ASO females, n=5 4wHF/ASO males. Comparisons between groups within each sex are shown. P values are calculated by a mixed-effects analysis with Šidák post-test comparing values during the intervention period (time points 27w-30w). **c-d,** *C3* expression is restricted to SMC-derived plaque cells. *C3* expression, TdTomato expression, and clustering in the 4-week (**c**) and 12-week (**d**) regression experiments are shown. Cells are from atherosclerotic aortic arches after removal of the adventitia, but a small group of fibroblasts is present in 12-week regression experiment data. Within plaque (i.e., not considering fibroblasts), *C3* is selectively expressed in modulated SMC-derived cells. Color coding within the SMC-derived cells corresponds to the main text (light blue = SMC0, dark blue = fibromyocytes, light brown = chondromyocytes, light green = SMC1/cap, light red = SMC2). The cells shown are after doublet removal.

Extended Data Fig. 8. Expression of genes encoding the TNF and IL1β receptors in SMC-derived cells. a-b, Expression of *Tnfrsf1a*, encoding the TNF receptor 1, and *Il1r1*, encoding the IL1β receptor, in clusters C0-C4 in the 4-week (**a**) and 12-week (**b**) regression experiments. *Tnfrsf1a* and *Il1r1* are expressed in SMC-derived cells with the highest expression in fibromyocytes and chondromyocytes. There is a trend towards lower expression of *Tnfrsf1a* after ApoB-LP lowering, which, however, did not reach genome-wide significance.

Extended Data Fig. 9. Validation of the RNA sequencing experiment. a-b, To validate the RNA sequencing experiment, we performed independent quantitative real-time PCR experiments in primary mouse aortic SMCs treated with cholesterol loading (chol, 10 μg/ml, 72 h) (**a**) or tumor necrosis factor (TNF, 10 ng/ml, 24 h) (**b**). Additionally, cells were treated with either a control siRNA (siCtr) or a *Ikbkb* siRNA (si*Ikbkb*). The expression levels of *C3*, *Lcn2*, *Vcam1*, and *Il6* genes are shown. We used three independent replicates per condition. Data are presented as mean±SEM. P values calculated by one-way ANOVA followed by Šidák post-test.

Extended Data Fig. 10. Graphical abstract. In this study, we combined smooth muscle cell (SMC) lineage-tracing, mouse models of atherosclerosis, techniques to manipulate lipoprotein metabolism, and single-cell expression profiling. We found that lowering ApoB-containing lipoproteins (ApoB-LPs) leads to early reversal of NFκB signaling in SMC-derived fibromyocytes and chondromyocytes, followed by their depletion from plaques. ASO, antisense oligonucleotides. rAAV-PCSK9, recombinant adeno-associated virus encoding proprotein convertase subtilisin/kexin type 9.

References

1. Borén, J. & Williams, K. J. The central role of arterial retention of cholesterol-rich apolipoprotein-B-containing lipoproteins in the pathogenesis of atherosclerosis: a triumph of simplicity. *Curr Opin Lipidol* **27**, 473–483 (2016).
2. Bartels, E. D., Christoffersen, C., Lindholm, M. W. & Nielsen, L. B. Altered metabolism of LDL in the arterial wall precedes atherosclerosis regression. *Circ Res* **117**, 933–942 (2015).
3. Feig, J. E. *et al.* Reversal of hyperlipidemia with a genetic switch favorably affects the content and inflammatory state of macrophages in atherosclerotic plaques. *Circulation* **123**, 989–998 (2011).
4. Peled, M. *et al.* A wild-type mouse-based model for the regression of inflammation in atherosclerosis. *PLoS ONE* **12**, e0173975 (2017).
5. Lin, J.-D. *et al.* Single-cell analysis of fate-mapped macrophages reveals heterogeneity, including stem-like properties, during atherosclerosis progression and regression. *JCI Insight* **4**, e124574, 124574 (2019).
6. Sharma, M. *et al.* Regulatory T Cells License Macrophage Pro-Resolving Functions During Atherosclerosis Regression. *Circ Res* **127**, 335–353 (2020).
7. Ridker, P. M. *et al.* Antiinflammatory Therapy with Canakinumab for Atherosclerotic Disease. *N Engl J Med* **377**, 1119–1131 (2017).
8. Tardif, J.-C. *et al.* Efficacy and Safety of Low-Dose Colchicine after Myocardial Infarction. *N Engl J Med* **381**, 2497–2505 (2019).
9. Feil, S., Hofmann, F. & Feil, R. SM22alpha modulates vascular smooth muscle cell phenotype during atherogenesis. *Circ Res* **94**, 863–865 (2004).
10. Shankman, L. S. *et al.* KLF4-dependent phenotypic modulation of smooth muscle cells has a key role in atherosclerotic plaque pathogenesis. *Nat Med* **21**, 628–637 (2015).
11. Jacobsen, K. *et al.* Diverse cellular architecture of atherosclerotic plaque derives from clonal expansion of a few medial SMCs. *JCI Insight* **2**, e95890 (2017).
12. Wirka, R. C. *et al.* Atheroprotective roles of smooth muscle cell phenotypic modulation and the TCF21 disease gene as revealed by single-cell analysis. *Nat Med* **25**, 1280–1289 (2019).
13. Kim, J. B. *et al.* Environment-Sensing Aryl Hydrocarbon Receptor Inhibits the Chondrogenic Fate of Modulated Smooth Muscle Cells in Atherosclerotic Lesions. *Circulation* **142**, 575–590 (2020).
14. Pan, H. *et al.* Single-Cell Genomics Reveals a Novel Cell State During Smooth Muscle Cell Phenotypic Switching and Potential Therapeutic Targets for Atherosclerosis in Mouse and Human. *Circulation* **142**, 2060–2075 (2020).
15. Wang, Y. *et al.* Smooth Muscle Cells Contribute the Majority of Foam Cells in ApoE (Apolipoprotein E)-Deficient Mouse Atherosclerosis. *Arterioscler Thromb Vasc Biol* **39**, 876–887 (2019).
16. Miano, J. M., Fisher, E. A. & Majesky, M. W. Fate and State of Vascular Smooth Muscle Cells in Atherosclerosis. *Circulation* **143**, 2110–2116 (2021).
17. Stegemann, C. *et al.* Comparative lipidomics profiling of human atherosclerotic plaques. *Circ Cardiovasc Genet* **4**, 232–242 (2011).
18. Dang, D. *et al.* Computational Approach to Identifying Universal Macrophage Biomarkers. *Front Physiol* **11**, 275 (2020).
19. Gayoso, A. & Shor, J. JonathanShor/DoubletDetection: doubletdetection v4.2. (2022) doi:10.5281/ZENODO.6349517.
20. van den Brink, S. C. *et al.* Single-cell sequencing reveals dissociation-induced gene expression in tissue subpopulations. *Nat Methods* **14**, 935–936 (2017).

21. Dobnikar, L. *et al.* Disease-relevant transcriptional signatures identified in individual smooth muscle cells from healthy mouse vessels. *Nat Commun* **9**, 4567 (2018).
22. Alencar, G. F. *et al.* Stem Cell Pluripotency Genes Klf4 and Oct4 Regulate Complex SMC Phenotypic Changes Critical in Late-Stage Atherosclerotic Lesion Pathogenesis. *Circulation* **142**, 2045–2059 (2020).
23. Aibar, S. *et al.* SCENIC: single-cell regulatory network inference and clustering. *Nat Methods* **14**, 1083–1086 (2017).
24. Newman, A. A. C. *et al.* Multiple cell types contribute to the atherosclerotic lesion fibrous cap by PDGFRβ and bioenergetic mechanisms. *Nat Metab* **3**, 166–181 (2021).
25. Björkegren, J. L. M. *et al.* Plasma Cholesterol–Induced Lesion Networks Activated before Regression of Early, Mature, and Advanced Atherosclerosis. *PLoS Genet* **10**, e1004201 (2014).
26. Wang, Z. *et al.* Myocardin and ternary complex factors compete for SRF to control smooth muscle gene expression. *Nature* **428**, 185–189 (2004).
27. Liu, Y. *et al.* Kruppel-like factor 4 abrogates myocardin-induced activation of smooth muscle gene expression. *J Biol Chem* **280**, 9719–9727 (2005).
28. Tang, R.-H. *et al.* Myocardin inhibits cellular proliferation by inhibiting NF-kappaB(p65)-dependent cell cycle progression. *Proc Natl Acad Sci U S A* **105**, 3362–3367 (2008).
29. Vengrenyuk, Y. *et al.* Cholesterol loading reprograms the microRNA-143/145-myocardin axis to convert aortic smooth muscle cells to a dysfunctional macrophage-like phenotype. *Arterioscler Thromb Vasc Biol* **35**, 535–546 (2015).
30. Wang, Y. *et al.* Dynamic changes in chromatin accessibility are associated with the atherogenic transitioning of vascular smooth muscle cells. *Cardiovasc Res* **118**, 2792–2804 (2022).
31. Turner, A. W. *et al.* Single-nucleus chromatin accessibility profiling highlights regulatory mechanisms of coronary artery disease risk. *Nat Genet* **54**, 804–816 (2022).
32. Cartwright, T., Perkins, N. D. & L Wilson, C. NFKB1: a suppressor of inflammation, ageing and cancer. *FEBS J* **283**, 1812–1822 (2016).
33. Rong, J. X., Shapiro, M., Trogan, E. & Fisher, E. A. Transdifferentiation of mouse aortic smooth muscle cells to a macrophage-like state after cholesterol loading. *Proc Natl Acad Sci U S A* **100**, 13531–13536 (2003).
34. Feig, J. E. *et al.* Regression of Atherosclerosis Is Characterized by Broad Changes in the Plaque Macrophage Transcriptome. *PLoS ONE* **7**, e39790 (2012).
35. von Scheidt, M. *et al.* Applications and Limitations of Mouse Models for Understanding Human Atherosclerosis. *Cell Metab* **25**, 248–261 (2017).
36. Aragam, K. G. *et al.* Discovery and systematic characterization of risk variants and genes for coronary artery disease in over a million participants. *Nat Genet* **54**, 1803–1815 (2022).
37. Räber, L. *et al.* Effect of Alirocumab Added to High-Intensity Statin Therapy on Coronary Atherosclerosis in Patients With Acute Myocardial Infarction: The PACMAN-AMI Randomized Clinical Trial. *JAMA* **327**, 1771 (2022).
38. Schwartz, G. G. *et al.* Alirocumab and Cardiovascular Outcomes after Acute Coronary Syndrome. *N Engl J Med* **379**, 2097–2107 (2018).
39. Martos-Rodríguez, C. J. *et al.* Fibrous Caps in Atherosclerosis Form by Notch-Dependent Mechanisms Common to Arterial Media Development. *Arterioscler Thromb Vasc Biol* **41**, e427–e439 (2021).
40. Alonso-Herranz, L., Albarrán-Juárez, J. & Bentzon, J. F. Mechanisms of fibrous cap formation in atherosclerosis. *Front Cardiovasc Med* **10**, 1254114 (2023).
41. Bennett, M. R., Sinha, S. & Owens, G. K. Vascular Smooth Muscle Cells in Atherosclerosis. *Circ Res* **118**, 692–702 (2016).

42. Gomez, D. *et al.* Interleukin-1β has atheroprotective effects in advanced atherosclerotic lesions of mice. *Nat Med* **24**, 1418–1429 (2018).
43. Brignall, R., Moody, A. T., Mathew, S. & Gaudet, S. Considering Abundance, Affinity, and Binding Site Availability in the NF-κB Target Selection Puzzle. *Front Immunol* **10**, 609 (2019).
44. Evrard, S. M. *et al.* Endothelial to mesenchymal transition is common in atherosclerotic lesions and is associated with plaque instability. *Nat Commun* **7**, 11853 (2016).
45. Sui, Y. *et al.* IKKβ links vascular inflammation to obesity and atherosclerosis. *J Exp Med* **211**, 869–886 (2014).
46. Otsuka, F., Sakakura, K., Yahagi, K., Joner, M. & Virmani, R. Has our understanding of calcification in human coronary atherosclerosis progressed? *Arterioscler Thromb Vasc Biol* **34**, 724–736 (2014).
47. Kessler, T. *et al.* Functional Characterization of the *GUCY1A3* Coronary Artery Disease Risk Locus. *Circulation* **136**, 476–489 (2017).
48. Bizet, A. A. *et al.* CD109-mediated degradation of TGF-β receptors and inhibition of TGF-β responses involve regulation of SMAD7 and Smurf2 localization and function. *J Cell Biochem* **113**, 238–246 (2012).
49. Bindesbøll, C. *et al.* NBEAL1 controls SREBP2 processing and cholesterol metabolism and is a susceptibility locus for coronary artery disease. *Sci Rep* **10**, 4528 (2020).
50. Schindelin, J. *et al.* Fiji: an open-source platform for biological-image analysis. *Nat Methods* **9**, 676–682 (2012).
51. McCarthy, D. J., Campbell, K. R., Lun, A. T. L. & Wills, Q. F. Scater: pre-processing, quality control, normalization and visualization of single-cell RNA-seq data in R. *Bioinformatics* **33**, 1179–1186 (2017).
52. Stuart, T. *et al.* Comprehensive Integration of Single-Cell Data. *Cell* **177**, 1888-1902.e21 (2019).
53. Stuart, T., Srivastava, A., Madad, S., Lareau, C. A. & Satija, R. Single-cell chromatin state analysis with Signac. *Nat Methods* **18**, 1333–1341 (2021).
54. Granja, J. M. *et al.* ArchR is a scalable software package for integrative single-cell chromatin accessibility analysis. *Nat Genet* **53**, 403–411 (2021).
55. Fornes, O. *et al.* JASPAR 2020: update of the open-access database of transcription factor binding profiles. *Nucleic Acids Res* **48**, D87–D92 (2020).
56. Schep, A. N., Wu, B., Buenrostro, J. D. & Greenleaf, W. J. chromVAR: inferring transcription-factor-associated accessibility from single-cell epigenomic data. *Nat Methods* **14**, 975–978 (2017).
57. Ewels, P. A. *et al.* The nf-core framework for community-curated bioinformatics pipelines. *Nat Biotechnol* **38**, 276–278 (2020).
58. Soneson, C., Love, M. I. & Robinson, M. D. Differential analyses for RNA-seq: transcript-level estimates improve gene-level inferences. *F1000Res* **4**, 1521 (2016).
59. Love, M. I., Huber, W. & Anders, S. Moderated estimation of fold change and dispersion for RNA-seq data with DESeq2. *Genome Biol* **15**, 550 (2014).

Figure 1

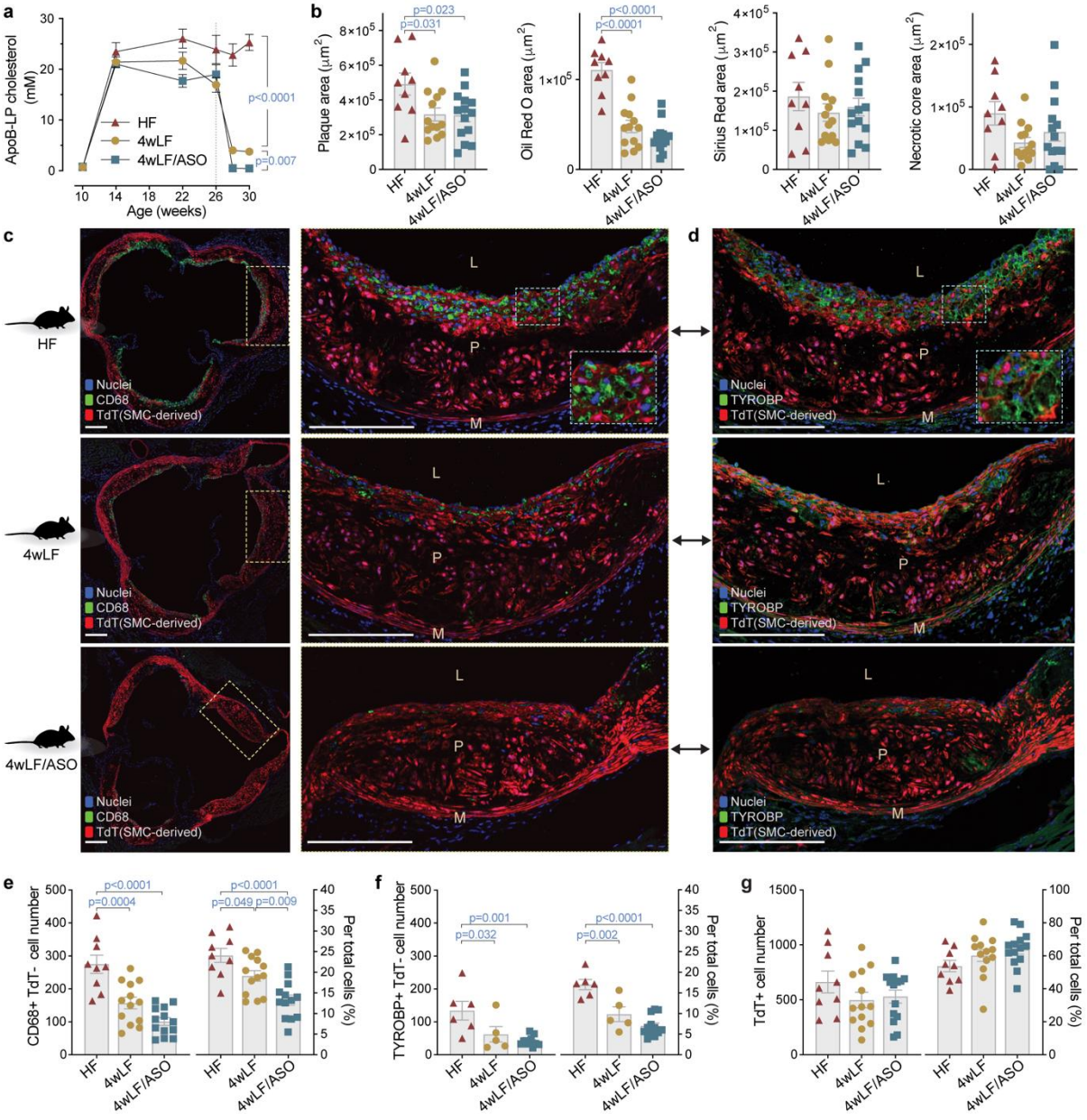
a
ApoB-LP cholesterol (mM)
Age (weeks)
HF
4wLF
4wLF/ASO
p<0.0001
p=0.007
b
Plaque area (μm²)
Oil Red O area (μm²)
Sirius Red area (μm²)
Necrotic core area (μm²)
p=0.023
p=0.031
p<0.0001
p<0.0001
c
d
Nuclei
CD68
TdT(SMC-derived)
TYROBP
L
P
M
e
CD68+ TdT- cell number
Per total cells (%)
p<0.0001
p=0.0004
p<0.0001
p=0.049
p=0.009
f
TYROBP+ TdT- cell number
p=0.001
p=0.032
p<0.0001
p=0.002
g
TdT+ cell number

Figure 2

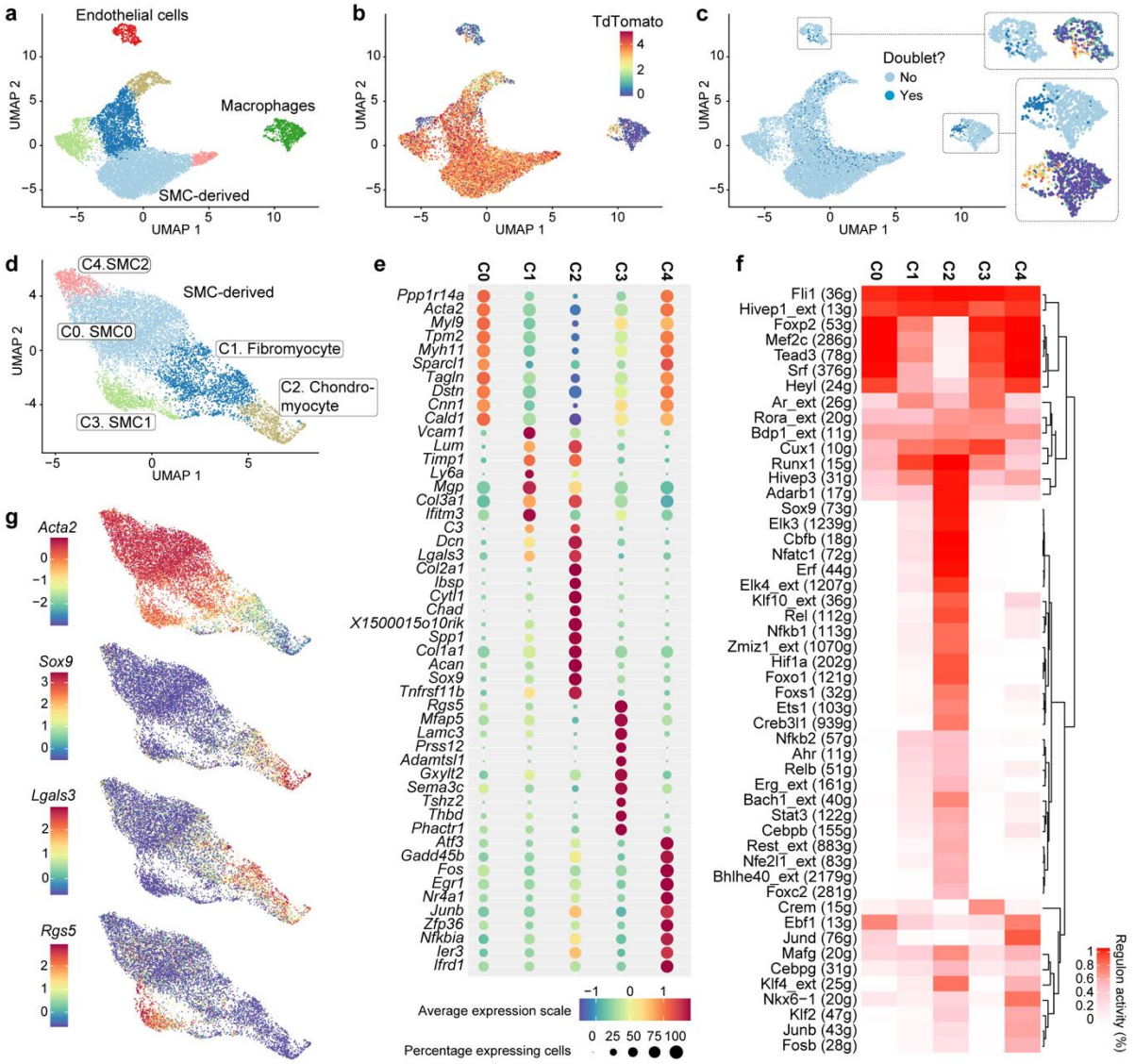
a
Endothelial cells
Macrophages
SMC-derived
UMAP 1
UMAP 2
b
TdTomato
c
Doublet?
No
Yes
d
C4.SMC2
SMC-derived
C0. SMC0
C1. Fibromyocyte
C2. Chondro-myocyte
C3. SMC1
e
C0
C1
C2
C3
C4
Ppp1r14a
Acta2
Myl9
Tpm2
Myh11
Sparcl1
Tagln
Dstn
Cnn1
Cald1
Vcam1
Lum
Timp1
Ly6a
Mgp
Col3a1
Ifitm3
C3
Dcn
Lgals3
Col2a1
Ibsp
Cytl1
Chad
X1500015o10rik
Spp1
Col1a1
Acan
Sox9
Tnfrsf11b
Rgs5
Mfap5
Lamc3
Prss12
Adamtsl1
Gxylt2
Sema3c
Tshz2
Thbd
Phactr1
Atf3
Gadd45b
Fos
Egr1
Nr4a1
Junb
Zfp36
Nfkbia
Ier3
Ifrd1
Average expression scale
Percentage expressing cells
f
Fli1 (36g)
Hivep1_ext (13g)
Foxp2 (53g)
Mef2c (286g)
Tead3 (78g)
Srf (376g)
Heyl (24g)
Ar_ext (26g)
Rora_ext (20g)
Bdp1_ext (11g)
Cux1 (10g)
Runx1 (15g)
Hivep3 (31g)
Adarb1 (17g)
Sox9 (73g)
Elk3 (1239g)
Cbfb (18g)
Nfatc1 (72g)
Erf (44g)
Elk4_ext (1207g)
Klf10_ext (36g)
Rel (112g)
Nfkb1 (113g)
Zmiz1_ext (1070g)
Hif1a (202g)
Foxo1 (121g)
Foxs1 (32g)
Ets1 (103g)
Creb3l1 (939g)
Nfkb2 (57g)
Ahr (11g)
Relb (51g)
Erg_ext (161g)
Bach1_ext (40g)
Stat3 (122g)
Cebpb (155g)
Rest_ext (883g)
Nfe2l1_ext (83g)
Bhlhe40_ext (2179g)
Foxc2 (281g)
Crem (15g)
Ebf1 (13g)
Jund (76g)
Mafg (20g)
Cebpg (31g)
Klf4_ext (25g)
Nkx6−1 (20g)
Klf2 (47g)
Junb (43g)
Fosb (28g)
Regulon activity (%)
g
Acta2
Sox9
Lgals3
Rgs5

Figure 3

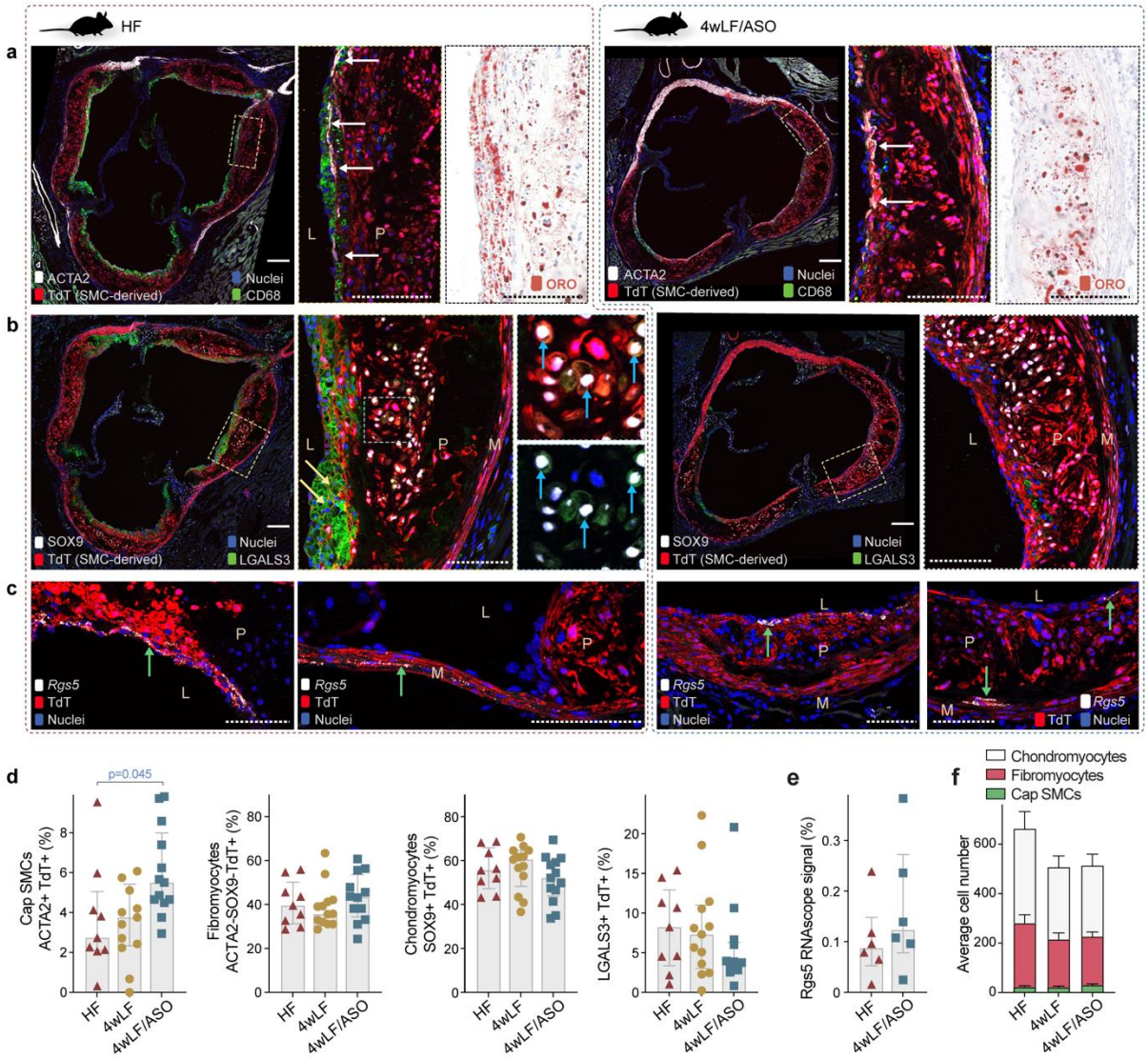
HF
4wLF/ASO
a
ACTA2
TdT (SMC-derived)
Nuclei
CD68
ORO
b
SOX9
LGALS3
c
Rgs5
TdT
Nuclei
d
p=0.045
Cap SMCs ACTA2+ TdT+ (%)
Fibromyocytes ACTA2-SOX9-TdT+ (%)
Chondromyocytes SOX9+ TdT+ (%)
LGALS3+ TdT+ (%)
e
Rgs5 RNAscope signal (%)
f
Chondromyocytes
Fibromyocytes
Cap SMCs
Average cell number
HF
4wLF
4wLF/ASO

Figure 4

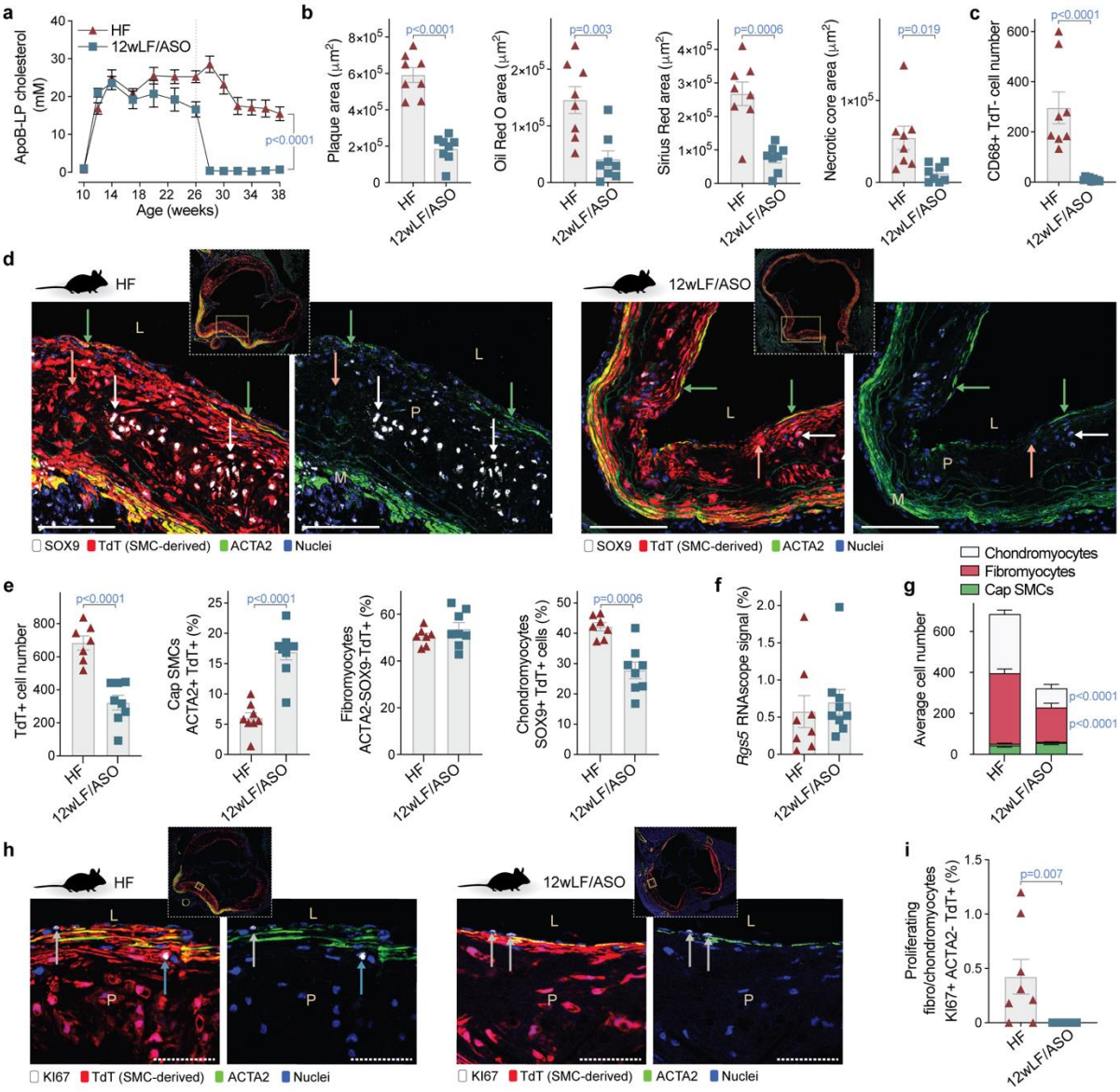
a
ApoB-LP cholesterol (mM)
HF
12wLF/ASO
p<0.0001
Age (weeks)
b
Plaque area (µm²)
Oil Red O area (µm²)
Sirius Red area (µm²)
Necrotic core area (µm²)
p<0.0001
p=0.003
p=0.0006
p=0.019
c
CD68+ TdT- cell number
p<0.0001
d
HF
12wLF/ASO
L
P
M
SOX9 TdT (SMC-derived) ACTA2 Nuclei
e
TdT+ cell number
Cap SMCs ACTA2+ TdT+ (%)
Fibromyocytes ACTA2-SOX9-TdT+ (%)
Chondromyocytes SOX9+ TdT+ cells (%)
p<0.0001
p=0.0006
f
Rgs5 RNAscope signal (%)
g
Chondromyocytes
Fibromyocytes
Cap SMCs
Average cell number
p<0.0001
p<0.0001
h
HF
12wLF/ASO
KI67 TdT (SMC-derived) ACTA2 Nuclei
i
Proliferating fibro/chondromyocytes KI67+ ACTA2- TdT+ (%)
p=0.007

Figure 5

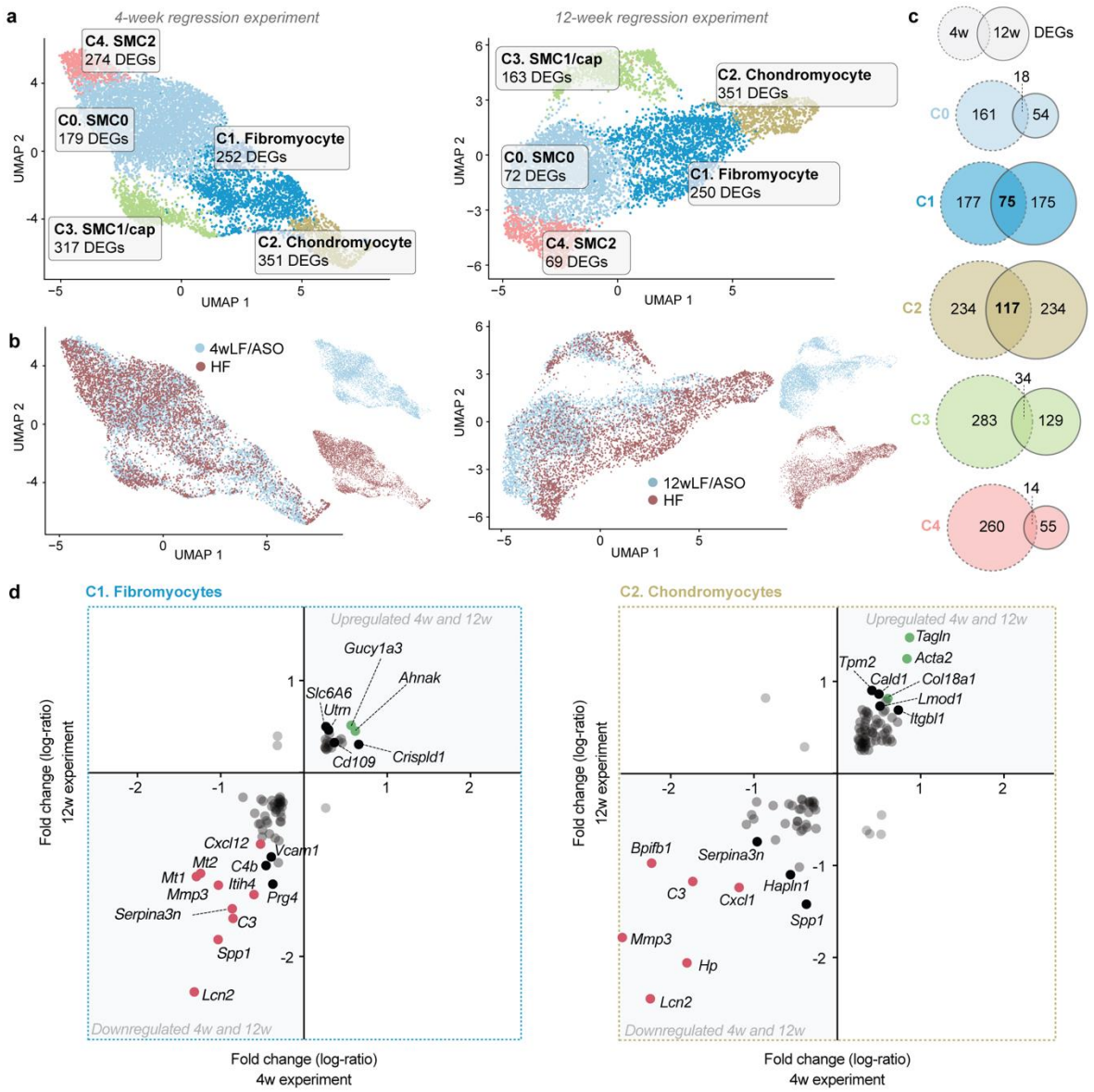
a
4-week regression experiment
C4. SMC2
274 DEGs
C0. SMC0
179 DEGs
C1. Fibromyocyte
252 DEGs
C3. SMC1/cap
317 DEGs
C2. Chondromyocyte
351 DEGs
12-week regression experiment
C3. SMC1/cap
163 DEGs
C2. Chondromyocyte
351 DEGs
C0. SMC0
72 DEGs
C1. Fibromyocyte
250 DEGs
C4. SMC2
69 DEGs
UMAP 1
UMAP 2
b
4wLF/ASO
HF
12wLF/ASO
HF
c
4w
12w
DEGs
C0
161
18
54
C1
177
75
175
C2
234
117
234
C3
283
34
129
C4
260
14
55
d
C1. Fibromyocytes
Upregulated 4w and 12w
Gucy1a3
Ahnak
Slc6A6
Utrn
Cd109
Crispld1
Cxcl12
Vcam1
Mt2
C4b
Mt1
Itih4
Mmp3
Prg4
Serpina3n
C3
Spp1
Lcn2
Downregulated 4w and 12w
Fold change (log-ratio)
12w experiment
Fold change (log-ratio)
4w experiment
C2. Chondromyocytes
Upregulated 4w and 12w
Tagln
Acta2
Tpm2
Cald1
Col18a1
Lmod1
Itgbl1
Bpifb1
Serpina3n
C3
Cxcl1
Hapln1
Spp1
Mmp3
Hp
Lcn2
Downregulated 4w and 12w
Fold change (log-ratio)
12w experiment
Fold change (log-ratio)
4w experiment

Figure 6

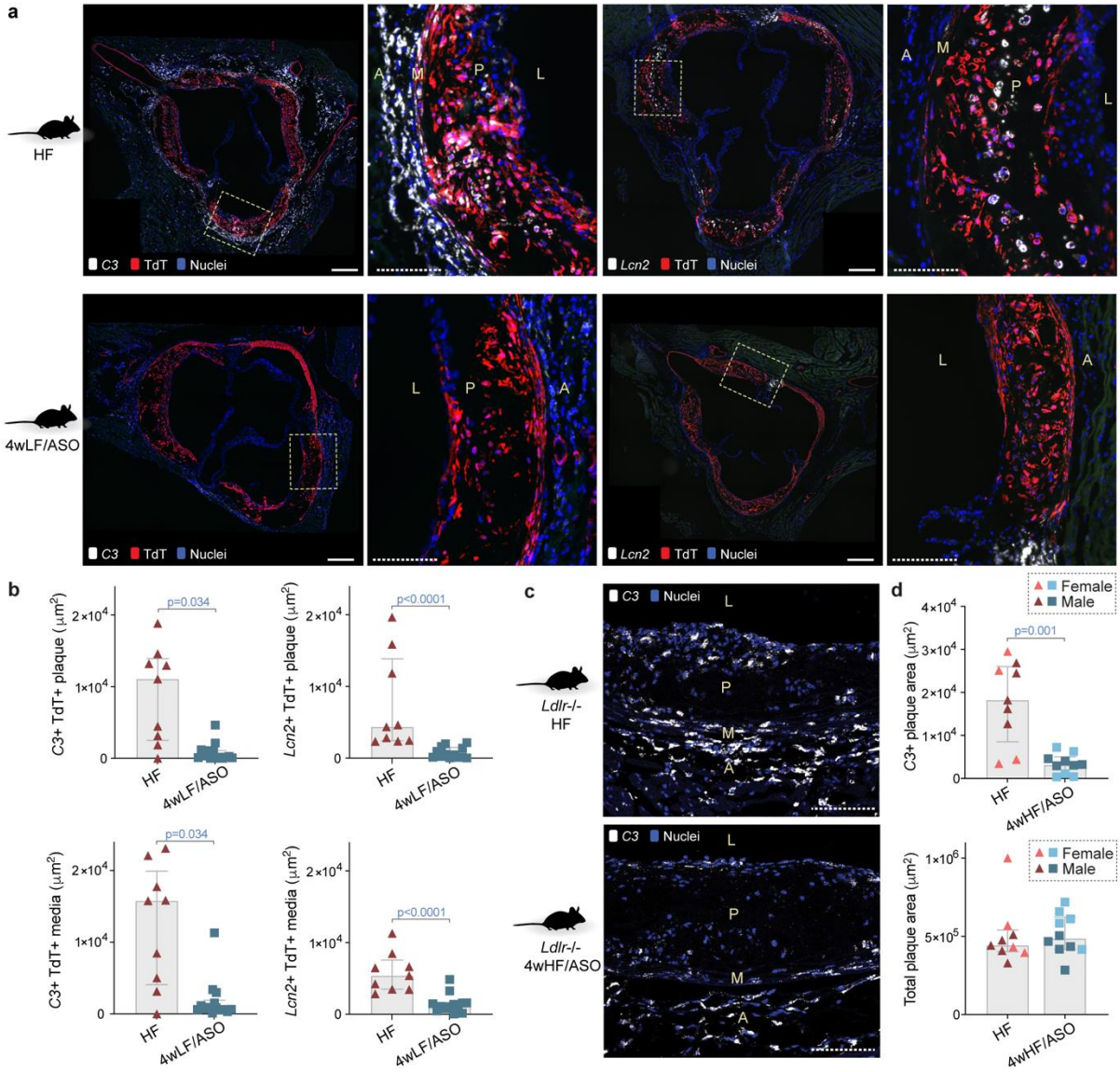
a
HF
4wLF/ASO
C3 TdT Nuclei
Lcn2 TdT Nuclei
A
M
P
L
b
C3+ TdT+ plaque (μm²)
Lcn2+ TdT+ plaque (μm²)
C3+ TdT+ media (μm²)
Lcn2+ TdT+ media (μm²)
p=0.034
p<0.0001
HF
4wLF/ASO
c
Ldlr-/-
HF
Ldlr-/-
4wHF/ASO
C3 Nuclei
d
Female
Male
C3+ plaque area (μm²)
Total plaque area (μm²)
p=0.001
4wHF/ASO

Figure 7

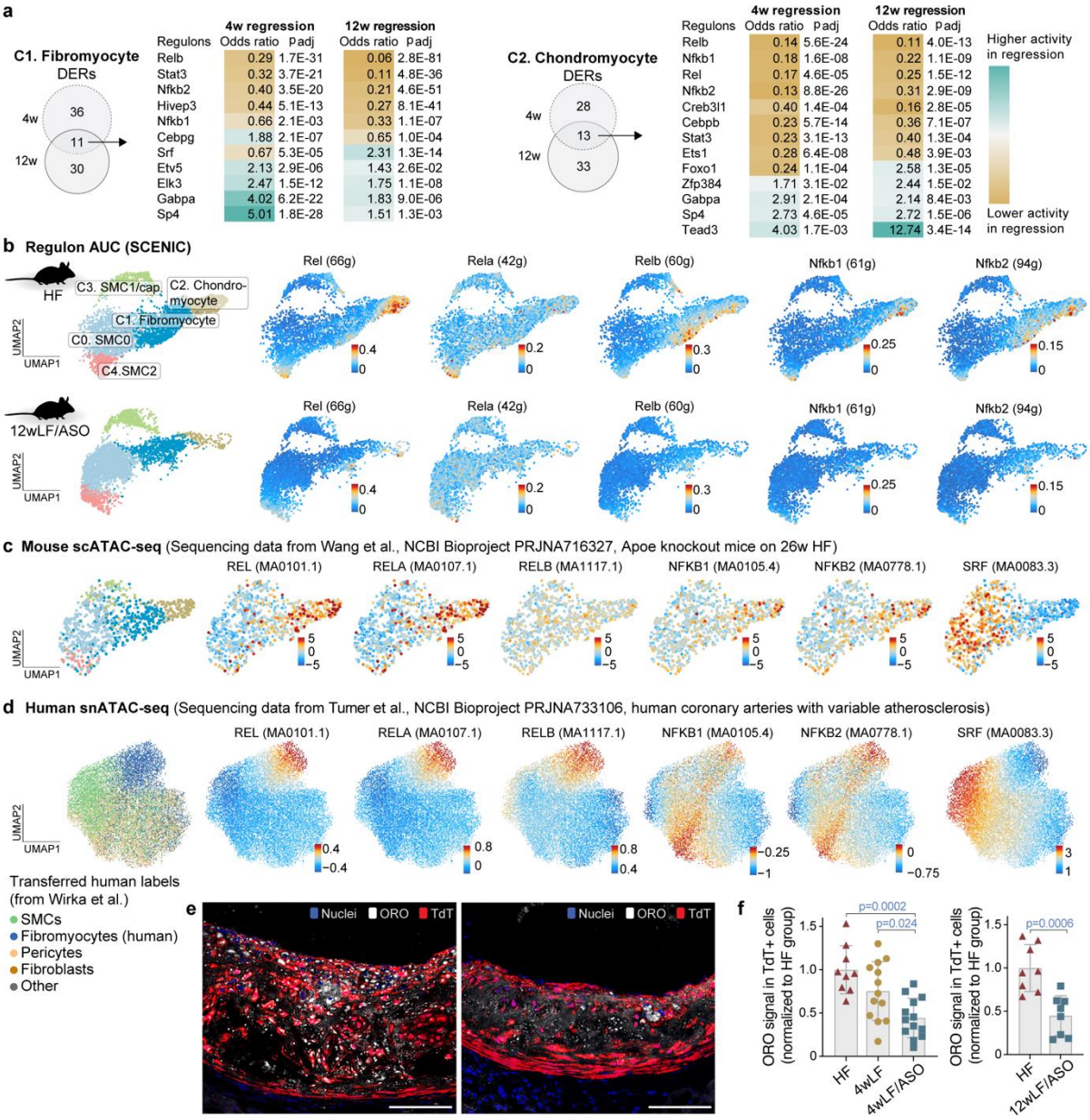
a
C1. Fibromyocyte DERs
4w
12w
36
11
30
Regulons
4w regression Odds ratio Padj
12w regression Odds ratio Padj
Relb 0.29 1.7E-31 0.06 2.8E-81
Stat3 0.32 3.7E-21 0.11 4.8E-36
Nfkb2 0.40 3.5E-20 0.21 4.6E-51
Hivep3 0.44 5.1E-13 0.27 8.1E-41
Nfkb1 0.66 2.1E-03 0.33 1.1E-07
Cebpg 1.88 2.1E-07 0.65 1.0E-04
Srf 0.67 5.3E-05 2.31 1.3E-14
Etv5 2.13 2.9E-06 1.43 2.6E-02
Elk3 2.47 1.5E-12 1.75 1.1E-08
Gabpa 4.02 6.2E-22 1.83 9.0E-06
Sp4 5.01 1.8E-28 1.51 1.3E-03
C2. Chondromyocyte DERs
4w
12w
28
13
33
Regulons
4w regression Odds ratio Padj
12w regression Odds ratio Padj
Relb 0.14 5.6E-24 0.11 4.0E-13
Nfkb1 0.18 1.6E-08 0.22 1.1E-09
Rel 0.17 4.6E-05 0.25 1.5E-12
Nfkb2 0.13 8.8E-26 0.31 2.9E-09
Creb3l1 0.40 1.4E-04 0.16 2.8E-05
Cebpb 0.23 5.7E-14 0.36 7.1E-07
Stat3 0.23 3.1E-13 0.40 1.3E-04
Ets1 0.28 6.4E-08 0.48 3.9E-03
Foxo1 0.24 1.1E-04 2.58 1.3E-05
Zfp384 1.71 3.1E-02 2.44 1.5E-02
Gabpa 2.91 2.1E-04 2.14 8.4E-03
Sp4 2.73 4.6E-05 2.72 1.5E-06
Tead3 4.03 1.7E-03 12.74 3.4E-14
Higher activity in regression
Lower activity in regression
b Regulon AUC (SCENIC)
HF
C3. SMC1/cap.
C2. Chondro-myocyte
C1. Fibromyocyte
C0. SMC0
C4.SMC2
UMAP2
UMAP1
12wLF/ASO
Rel (66g)
Rela (42g)
Relb (60g)
Nfkb1 (61g)
Nfkb2 (94g)
c Mouse scATAC-seq (Sequencing data from Wang et al., NCBI Bioproject PRJNA716327, Apoe knockout mice on 26w HF)
REL (MA0101.1)
RELA (MA0107.1)
RELB (MA1117.1)
NFKB1 (MA0105.4)
NFKB2 (MA0778.1)
SRF (MA0083.3)
d Human snATAC-seq (Sequencing data from Turner et al., NCBI Bioproject PRJNA733106, human coronary arteries with variable atherosclerosis)
Transferred human labels (from Wirka et al.)
SMCs
Fibromyocytes (human)
Pericytes
Fibroblasts
Other
e
Nuclei ORO TdT
f
ORO signal in TdT+ cells (normalized to HF group)
p=0.0002
p=0.024
p=0.0006
HF
4wLF
4wLF/ASO
12wLF/ASO

Figure 8

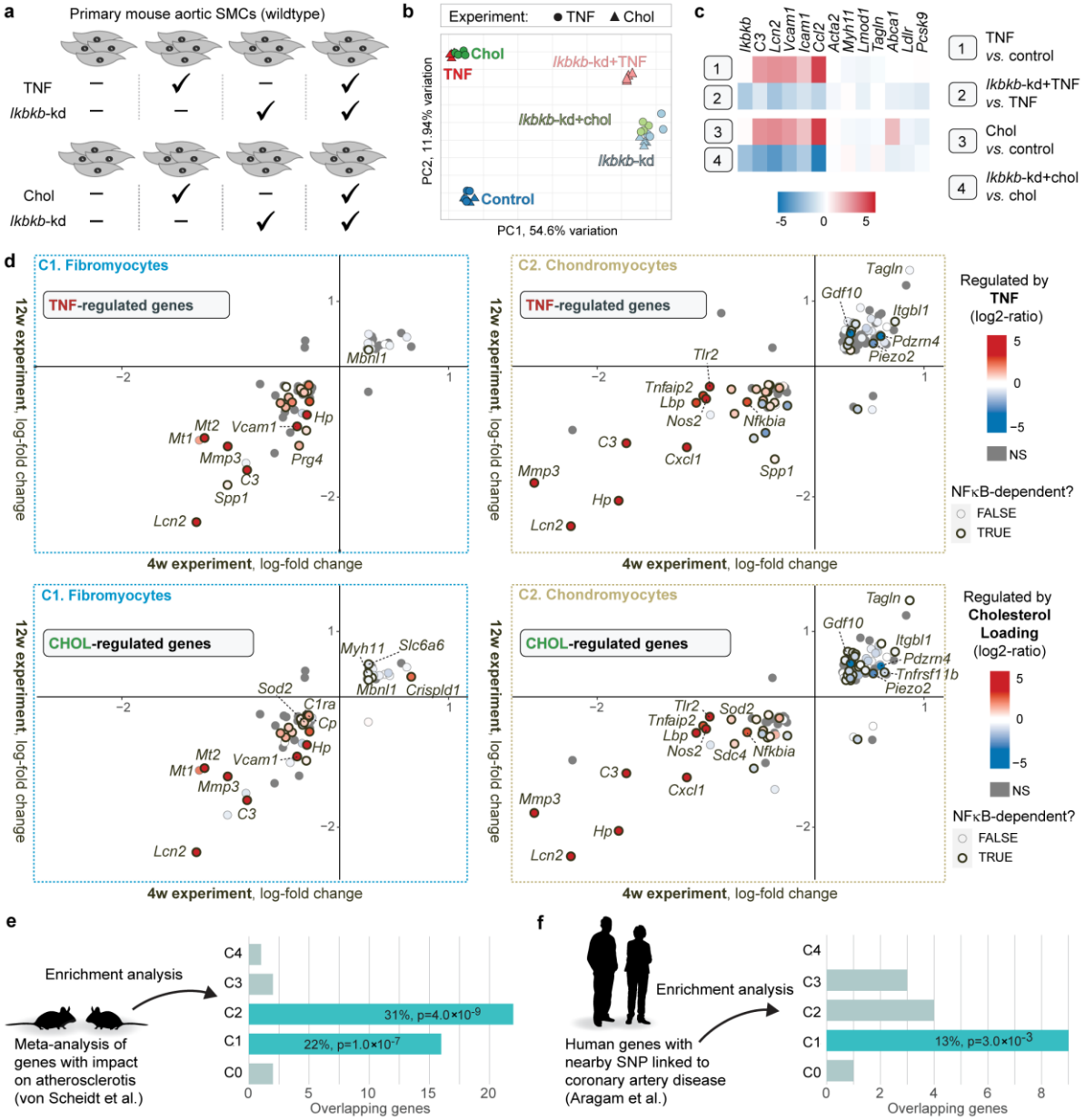
a
Primary mouse aortic SMCs (wildtype)
TNF
Ikbkb-kd
Chol
Ikbkb-kd
b
Experiment: TNF Chol
Chol
TNF
Ikbkb-kd+TNF
Ikbkb-kd+chol
Ikbkb-kd
Control
PC2, 11.94% variation
PC1, 54.6% variation
c
Ikbkb
C3
Lcn2
Vcam1
Icam1
Ccl2
Acta2
Myh11
Lmod1
Tagln
Abca1
Ldlr
Pcsk9
1 TNF vs. control
2 Ikbkb-kd+TNF vs. TNF
3 Chol vs. control
4 Ikbkb-kd+chol vs. chol
-5 0 5
d
C1. Fibromyocytes
TNF-regulated genes
12w experiment, log-fold change
4w experiment, log-fold change
Mbnl1
Mt2
Vcam1
Hp
Mt1
Mmp3
Prg4
C3
Spp1
Lcn2
C2. Chondromyocytes
TNF-regulated genes
Tagln
Gdf10
Itgbl1
Pdzrn4
Piezo2
Tlr2
Tnfaip2
Lbp
Nos2
Nfkbia
C3
Cxcl1
Mmp3
Spp1
Hp
Lcn2
Regulated by TNF (log2-ratio)
5
0
-5
NS
NFκB-dependent?
FALSE
TRUE
C1. Fibromyocytes
CHOL-regulated genes
Myh11
Slc6a6
Sod2
Mbnl1
Crispld1
C1ra
Cp
Hp
Mt2
Vcam1
Mt1
Mmp3
C3
Lcn2
C2. Chondromyocytes
CHOL-regulated genes
Tagln
Gdf10
Itgbl1
Pdzrn4
Tnfrsf11b
Piezo2
Tlr2
Sod2
Tnfaip2
Lbp
Nos2
Sdc4
Nfkbia
C3
Cxcl1
Mmp3
Hp
Lcn2
Regulated by Cholesterol Loading (log2-ratio)
5
0
-5
NS
NFκB-dependent?
FALSE
TRUE
e
Enrichment analysis
Meta-analysis of genes with impact on atherosclerotis (von Scheidt et al.)
C4
C3
C2
C1
C0
31%, p=4.0×10-9
22%, p=1.0×10-7
0 5 10 15 20
Overlapping genes
f
Enrichment analysis
Human genes with nearby SNP linked to coronary artery disease (Aragam et al.)
C4
C3
C2
C1
C0
13%, p=3.0×10-3
0 2 4 6 8
Overlapping genes

Extended Data Fig. 1

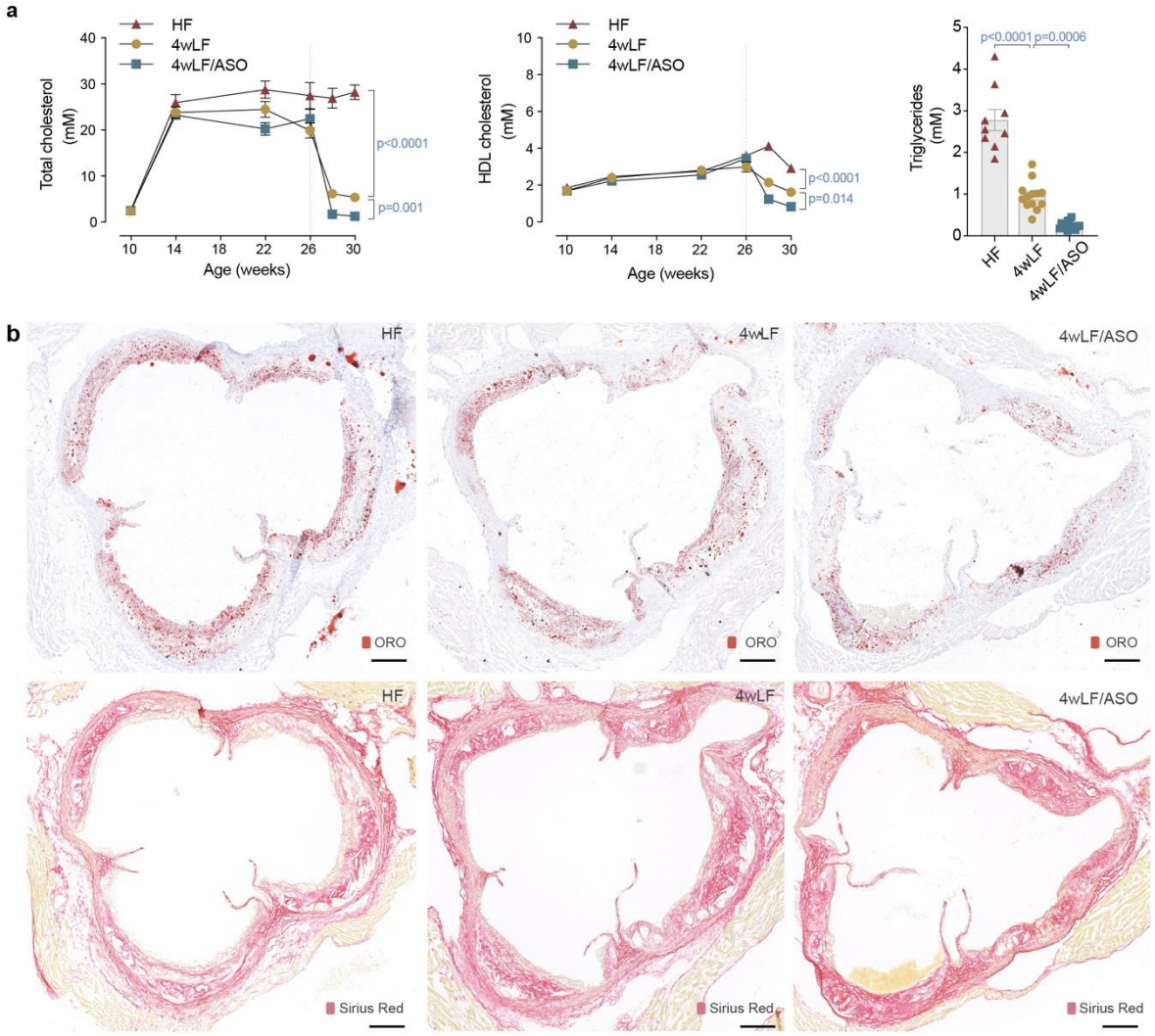

Extended Data Fig. 2

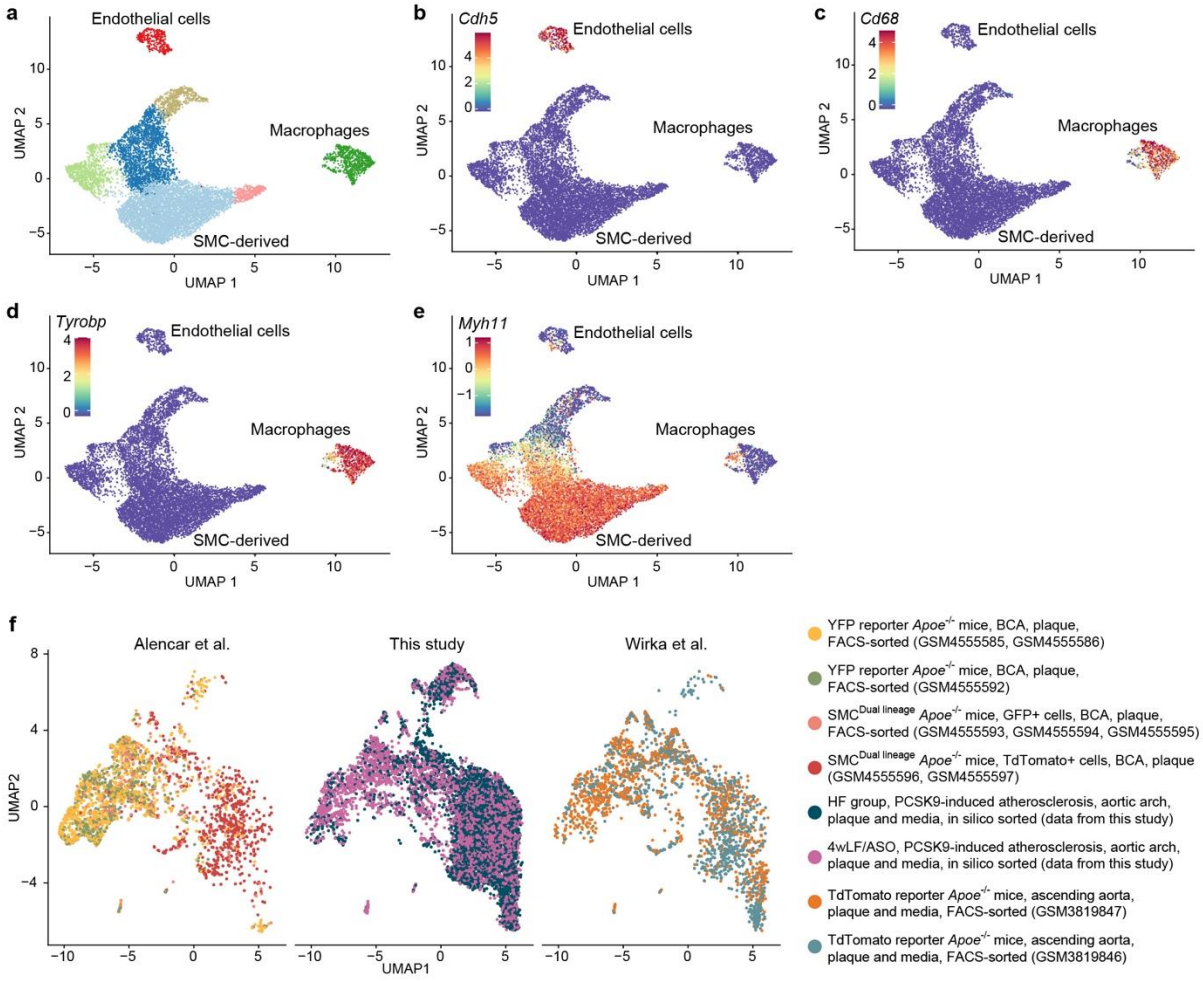

Extended Data Fig. 3

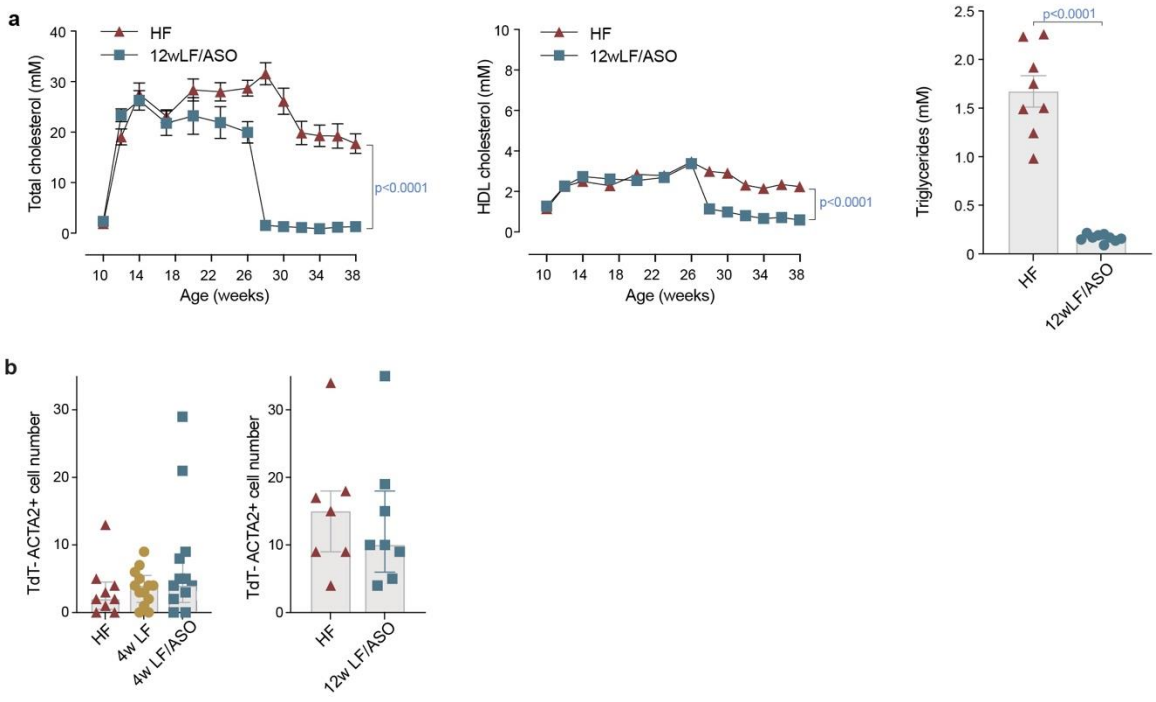

Extended Data Fig. 4

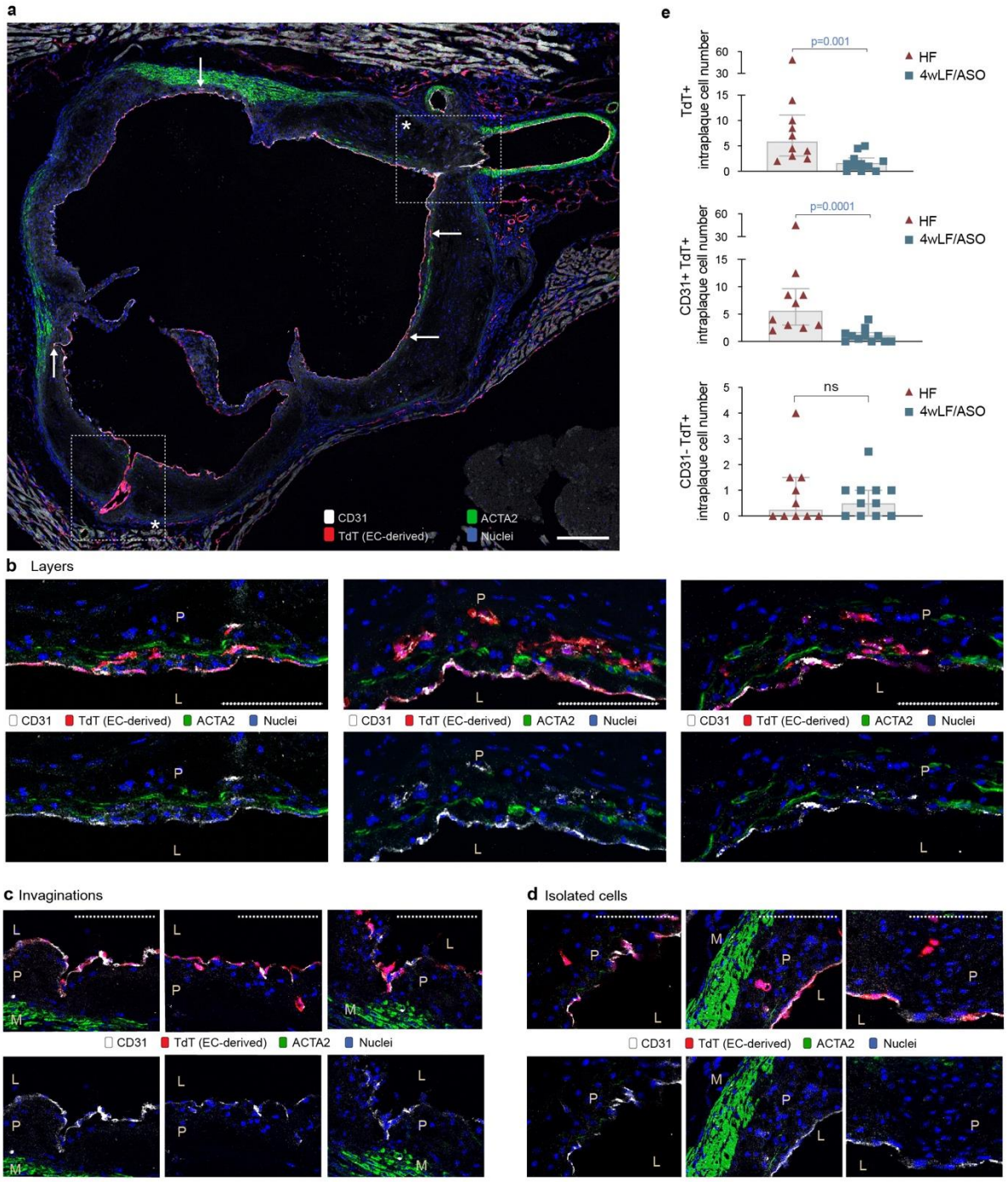

Extended Data Fig. 5

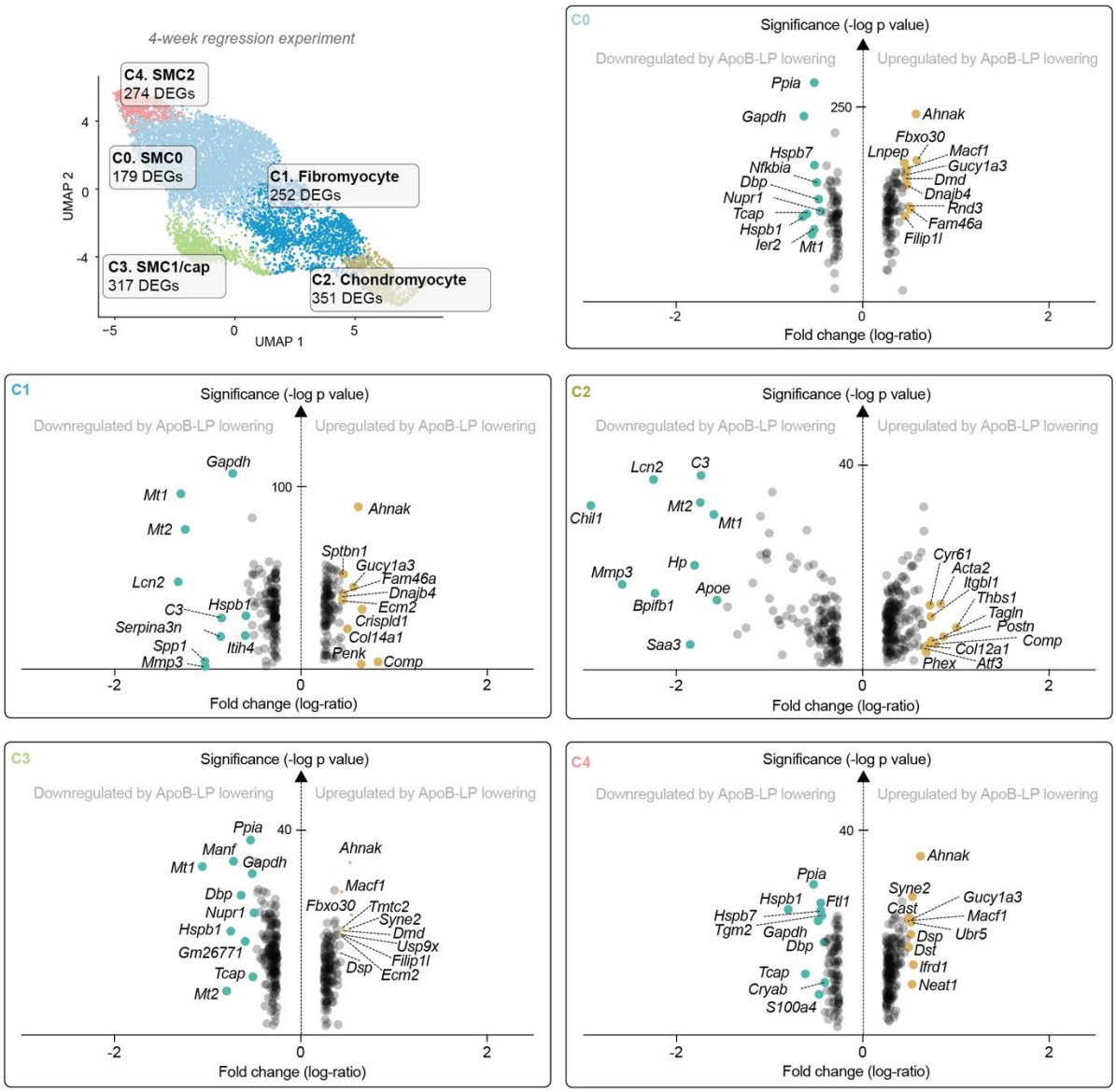

Extended Data Fig. 6

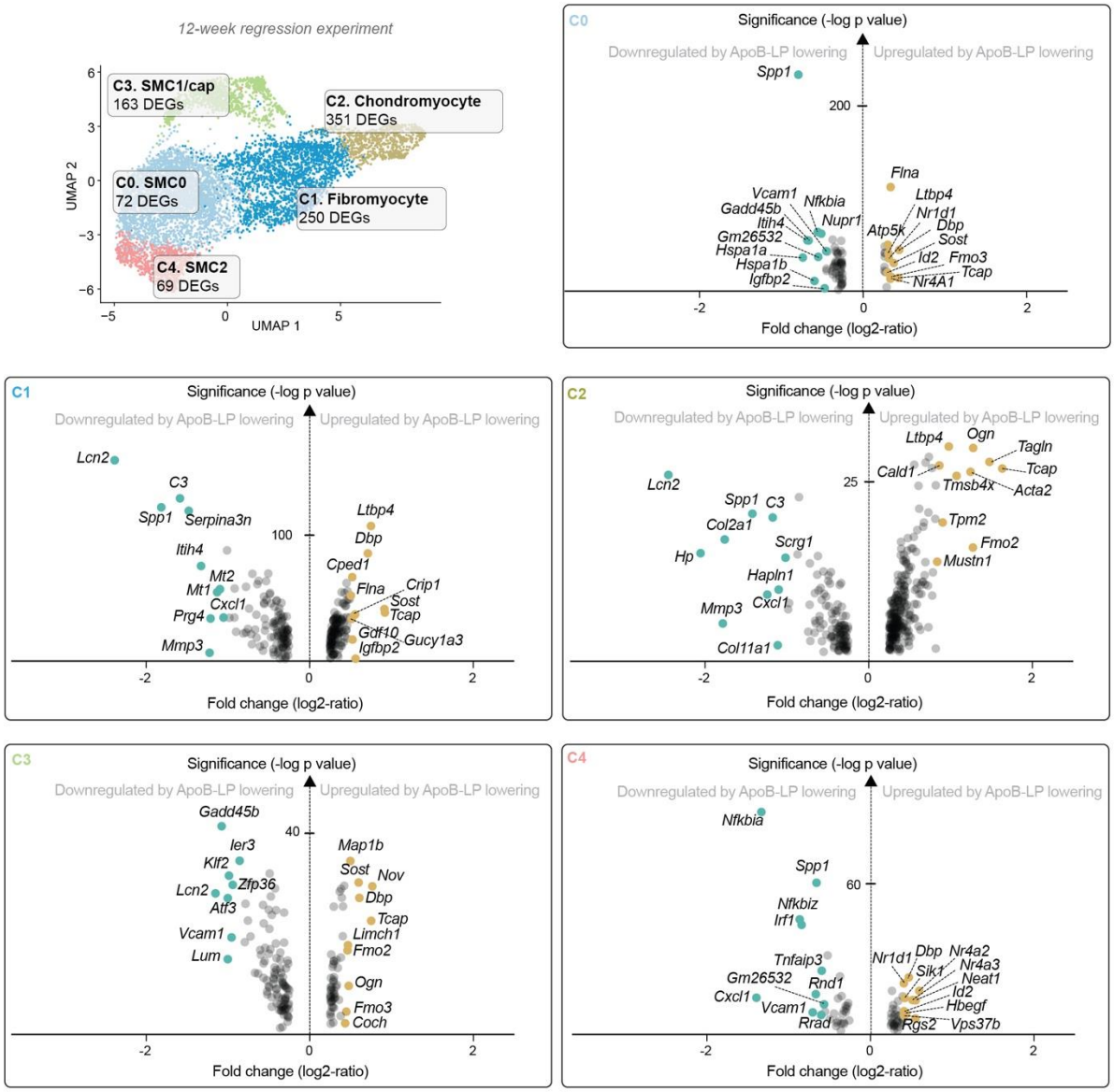

Extended Data Fig. 7

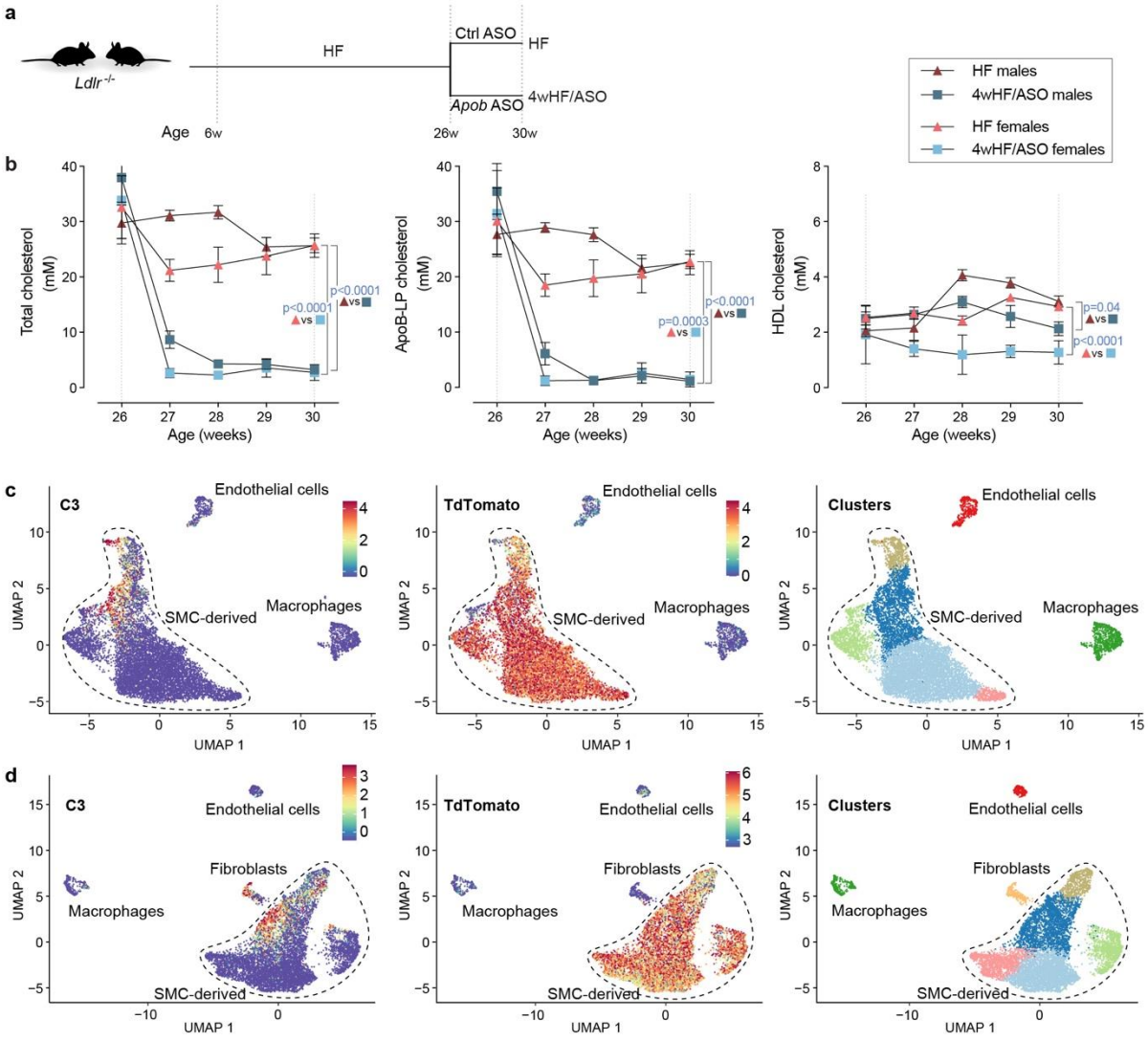

Extended Data Fig. 8

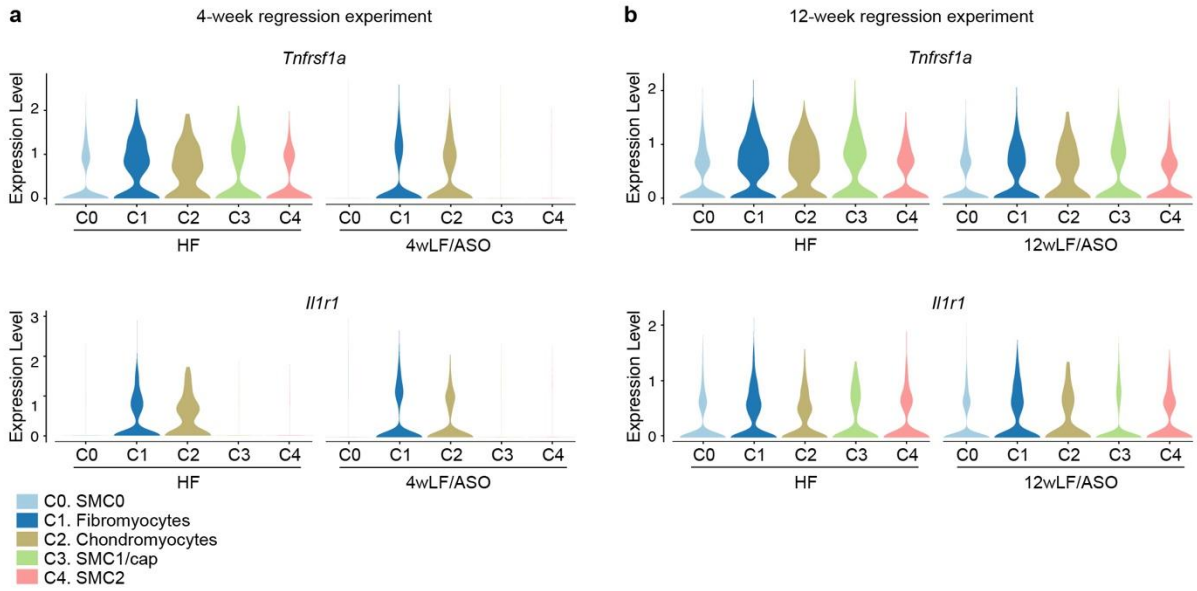

Extended Data Fig. 9

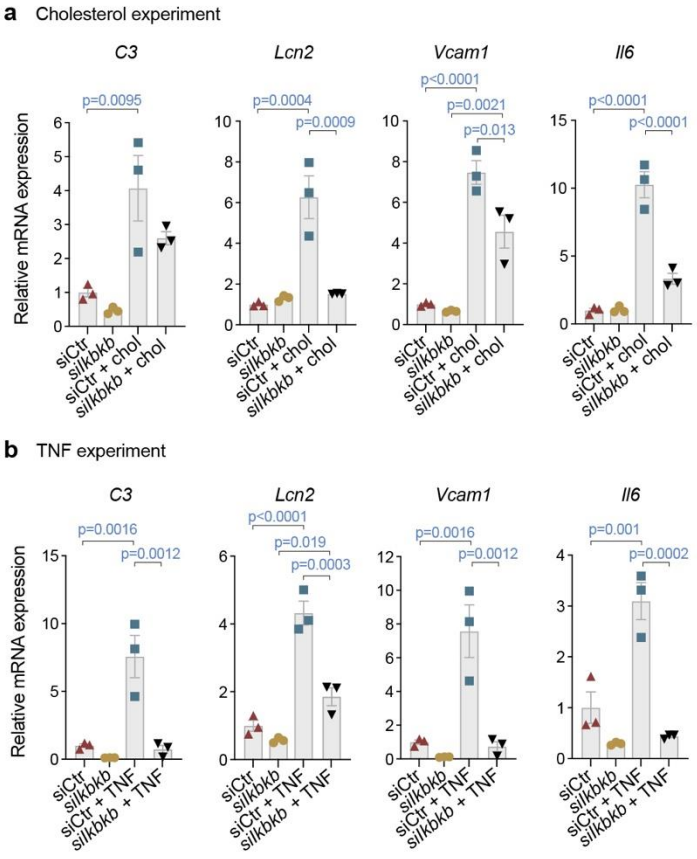

Extended Data Fig. 10